Chapter 3. **Flow around circular cylinders: state of the art**

This chapter describes the current state of knowledge of the flow around smooth and rough circular cylinders. The Reynolds number is the single governing parameter in disturbance-free flow around a two dimensional circular cylinder. Real flows are affected by a wide variety of disturbances, classified as influencing parameters. In particular, three dimensional effects have to be considered in view of the design of structures. They can be enhanced in atmospheric flow and depend on the aspect ratio.

3.1 The boundary layer and its separation

A body is classified as aerodynamically bluff – in opposite to streamlined – "when the flow streamlines do not follow the surface of the body, but detach from it leaving regions of separated flow and a wide trailing wake" (Cook, 1985). Circular cylinders belong to the class of bluff bodies with rounded shape, characterized by a separation point which can move and adjust itself in response to the flow structure in the separated region. In particular, separation will generally be delayed when transition from laminar to turbulent boundary layer occurs (Buresti, 2012). According to Zdravkovich (1997), the disturbed flow field around a circular cylinder can be divided into four regions: [1)] one narrow region of retarded flow close to stagnation; [2)] two boundary layers attached to the surface of the cylinder; [3)] two sidewise regions of displaced and accelerated flow; [4)] a wide downstream region of separated flow, called the wake. The near wake is initially bordered by the separated boundary layers which continue to develop downstream as free-shear layers. The concept of a thin boundary layer which develops around a body as a result of viscous friction was first presented by Prandtl in 1904. He evaluated the boundary layer thickness (δ) around circular cylinders at high Re as:

$$\delta \propto \frac{D}{\sqrt{\mathrm{Re}}} \tag{3.1}$$

The boundary layer has only a small thickness near the stagnation point and generally increases with distance along the surface. Zdravkovich (1997) uses a factor of proportionality equal to 5 at φ = 60°.

In the boundary layer, the velocity varies from the free stream value to zero at the wall, where fluid adheres to the boundary (no-slip condition). Therefore, a large velocity gradient exists normal to the surface and the shearing forces (which arise from the tangential shearing flow of the fluid along the surface of the body) are transmitted through the fluid shear layers adjacent to the surface. In the forward facing part of a circular cylinder, the flow accelerates and the boundary layers around the cylinder are subjected to a favorable (negative) pressure gradient. The region of accelerated flow is then followed by a small region of adverse (positive) pressure gradient before separation. In this decelerating flow region – over the rearward facing part of the body – the velocity at the edge of the boundary layer decreases. Due to the no-slip condition at the surface, at each value of z within the boundary layer the reduction of velocity in passing downstream varies from zero at the wall to a certain value at the edge of the boundary. There often comes a point at which the velocity gradient normal to the surface, at the surface, becomes zero. At this point, the viscous shear force must also be zero, which means that the boundary layer can no longer progress along the surface and thus separates. For this reason, the positive pressure gradient in the decelerating flow region is regarded as an adverse pressure gradient (ESDU 71012).
Downstream of the separation of the boundary layer, there is a region of reversed flow close to the surface. In fact, the region between the separated boundary layer and the surface is filled with an eddying flow in which the velocity and direction vary with time in an almost random manner and it has little or no relation to that of the free stream.

3.2 The state of the flow as a function of the Reynolds number

The state of the flow around a circular cylinder can be either fully laminar (at very low Re), fully turbulent (at very high Re, theoretically Re $\rightarrow \infty$, in practice it is limited by occurrence of compressibility effects in air) or there can be a transition from laminar to turbulent state either in the wake, in the free shear layers or in the boundary layers. In laminar flow, the adjacent fluid layers in the flow slide over each other and only friction forces act between them, without macroscopic mixing. Transition from laminar to turbulent flow was first discovered by Reynolds (1883) in a smooth pipe and then the concept was applied by Rayleigh (1896, 1915) to the flow around spheres and cylinders. In this case, the external diameter of the sphere or the circular cylinder was taken as the characteristic length. The Reynolds number is thus the governing parameter of the state of the flow. However, as stressed by Zdravkovich (1997), it is the single governing parameter only in disturbance-free flow. Real flows around

circular cylinders in most practical applications are affected by a wide variety of disturbances, which are classified as influencing parameters. Turbulence of the incoming flow, surface roughness, aspect ratio, end-effects (ground-wall effects and free-end effects), oscillations and wall-blockage are the most common influencing parameters. Transition is very sensitive to small disturbances, which may initiate transition at lower Re and in case become themselves governing parameters.
In this section, it is referred to an idealized disturbance-free flow, so that it is allowed to classify the flow regimes on the only basis of the Reynolds number (the aspect ratio is an ever-present influencing parameter, but – as clarified by Zdravkovich – it becomes a governing one only for a short cylinder with a free end).
The adverse pressure gradient reduces the skin friction to zero and at that instant the separation of the flow from the surface takes place. The capability of the boundary layer to sustain higher adverse pressure gradients before separation depends on the state of the flow and thus on the Reynolds number. The effect of mixing of fluid elements in a turbulent boundary layer promotes a greater interchange of momentum between layers which in turn increases the thickness δ of the boundary layer. Furthermore, the mixing process produces an effective shear stress which is additive to the shear stress produced by the viscosity of the fluid. As a consequence, the retarded fluid layers adjacent to the surface can be pulled further along the surface into regions of higher pressure. Because of that, the thick turbulent boundary layer is able to progress further against an unfavorable pressure gradient and it separates at a point further along a surface. Instead, in free-disturbance conditions, fully laminar boundary layers can only exist when the external pressure gradient is favorable. This is the reason for the early occurrence of laminar separation. As it will be showed in the following, a useful parameter which quantifies the capability of the flow to sustain the adverse pressure gradients prior to separation around a circular cylinder is the adverse pressure recovery. Its magnitude can be expressed by $C_{p,b} - C_{p,min}$, being $C_{p,b}$ and $C_{p,min}$ the base pressure coefficient (at $\varphi = 180°$) and the minimum pressure coefficient.

A first classification of the states of the flow around a smooth cylinder is proposed by Roshko (1961). Four regimes are defined: subcritical, critical, supercritical and transcritical. Later, Achenbach (1971) also referred to this classification for rough cylinders (section 3.3). In the subcritical state, there is an early laminar separation (angle of separation ≈ 70°-80°) and the drag is independent on Re. The critical regime is a range of transition between laminar and turbulent separation. It begins with the initial fall of the drag coefficient and ends with the formation of two laminar

separation bubbles at Re = Re_{cr}, which corresponds to the minimum drag. The supercritical range on smooth cylinders is still characterized by the two bubbles (rather constant low drag coefficient and narrow wake, with separation around 140°). After this first stable stage, the supercritical regime becomes unstable, with disruption of bubbles and suppression of vortex shedding. Roshko suggests that the disappearance of the bubbles marks the transition from supercritical to transcritical range, where the separation is purely turbulent and it occurs at lower angles (≈ 110°). Vortex shedding reappears in the transcritical range, it was discovered by Roshko and published for the first time in 1961.

According to Zdravkovich (1997), the position of the separation point (with regard to the position of transition from laminar to turbulent boundary layer) is the key feature to classify a particular state of the flow around a circular cylinder. He proposes a detailed classification based on occurrence of transition in different regions around the circular cylinder. It is reported in Table 3.1 and briefly explained in the following.

Table 3.1 Epitome of disturbance-free flow regimes (Zdravkovich, 1997)

STATE		REGIME		Re RANGES
L	LAMINAR	1	No-separation	0 to 4-5
		2	Closed wake	4-5 to 30-38
		3	Periodic wake	30-48 to 180-200
TrW	TRANSITION IN WAKE	1	Lower transition regime	180-200 to 220-250
		2	Upper transition regime	220-250 to 350-400
TrSL	TRANSITION IN SHEAR LAYERS	1	Lower subcritical	350-400 to $1*10^3$-$2*10^3$
		2	Intermediate subcritical	$1*10^3$-$2*10^3$ to $2*10^4$-$4*10^4$
		3	Upper subcritical	$2*10^4$-$4*10^4$ to $1*10^5$-$2*10^5$
TrBL	TRANSITION IN BOUNDARY LAYERS	0	Pre-critical	$1*10^5$-$2*10^5$ to $3*10^5$-$3.4*10^5$
		1	Single bubble	$3*10^5$-$3.4*10^5$ to $3.8*10^5$-$4*10^5$
		2	Two-bubble	$3.8*10^5$-$4*10^5$ to $5*10^5$-10^6
		3	Supercritical	$5*10^5$-10^6 to $3.5*10^6$-$6*10^6$
		4	Post-critical	$3.5*10^6$-$6*10^6$ to (?)
T	FULLY TURBULENT	1	Invariable	(?) to ∞
		2	Ultimate	

3.2.1 Fully laminar state

The fully laminar state (L, Re < 200) is characterized by three basic flow regimes. In the first one, the creeping flow regime (L1), separation does not occur because the

cylinder at extremely low Re (Re < 5) is dominated by viscous forces. Then, the magnitude of viscous forces decreases at higher Re and a steady separation initiates; the free shear layers meet at the end of the near-wake at the so-called confluence point. Thus, a laminar, closed, steady near-wake is formed behind the cylinder (L2). The well-known Von Karman eddy street starts with the instability of such an elongated closed near-wake which commences a sinusoidal oscillation for Re > 30-48. As Reynolds increases, the amplitude of the trail oscillations increases and the shear layers start to roll up at crests and troughs. That is, according to the nomenclature chosen by Zdravkovich, the flow regime L3. In such a shedding mode, initiated by the instability of the laminar wake, the laminar eddies are not shed starting from the cylinder, but they are formed gradually as they are carried downstream. Kovasznay (1949) writes: "it is remarkable that the fluctuations close to the cylinder are very small and that they develop the maximum intensity only in the vicinity of X/D = 7. Thus, the eddies are not shed starting from the cylinder at this low Re, but develop several diameters downstream". This mode is also identified as the low-speed mode, as opposite to the high-speed shedding mode of turbulent eddies which are shed starting from the cylinder itself at higher Re. Karman (1912) derived the first theoretical model by considering the stability of staggered vortices in two parallel rows. However, it was Bénard in 1908 the first who sketched the alternate procession of eddies observed in water.

3.2.2 Transitional states

All laminar flows undergo transition to turbulence above a certain Re. Around circular cylinders, it is interesting to describe the succession of transitions in various regions of the disturbed flow as Re increases. Zdravkovich (1997) identifies three different transitional stages of flow, based on the fact that transition may occur in the wake (TrW), in the shear layers (TrSL) and in the boundary layers (TrBL). Gerrard (1978) noted that all transition states are characterized by the appearance, development and disappearance of an entirely new flow structure. As it will be explained later, such flow structures are called fingers in TrW, transition waves in TrSL and separation bubbles in TrBL.

Transition in the wake

As Reynolds number increases, the laminar wake undergoes transition to turbulence (TrW, Re from 180-200 until 350-400), due to random initiation and growth of irregularities. The progressive distortion of laminar eddy filaments is described by Gerrard (1978) as the onset of "fingers" at randomly disposed spanwise positions. The

name "fingers" describes the fact that such a distortion of filaments always points toward the cylinder.

In the so-called lower transition regime (TrW1), the eddies are formed laminar and become turbulent further downstream. Then, transition spreads gradually upstream with increasing Re, until the eddies become turbulent during its formation (TrW2). According to Gerrard (1978), it is the mixing with the free stream around the eddies that promotes the formation of turbulent eddies.

The key feature of this transitional state is the change of the shedding mode from low-speed mode (which characterizes L3 and TrW1) to high-speed mode, which appears in TrW2. This change – that represents the boundary between TrW1 and TrW2 – is marked by a jump in the Strouhal number. It has been measured at Re ≈ 250 by Roshko, (1954) and it distinguishes two different S_t-versus-Re curves, for the two shedding modes, respectively: while in L3 and TrW1 (low-speed mode) S_t increases with Re, later on S_t is almost constant with rising Re. Anyway, the transition from low- to high-speed mode of eddy shedding is not smooth and an overlapping of the two modes of shedding (two peaks in the frequency spectra) has also been argued (Zdravkovich, 1992).

The characteristic feature of the high-speed mode (Gerrard, 1966) is that the growth of an eddy on one side of the cylinder (in an almost stationary position) induces transverse flow across the wake, which is responsible for the cut-off of the subsequent eddy from a further supply of circulation. It is at this stage, and because of the shear layer crossing the wake, that the eddy is shed from the cylinder.

Transition in the shear layer

After transition in the wake, at higher Re, transition occurs in the shear-layer, TrSL (Re from 350-400 until $1\text{-}2*10^5$). Basically, it is the usually called subcritical flow state, meaning that the boundary layer remains laminar up to and beyond separation. In this state, the free shear layers which surround the near-wake are initially laminar but they become turbulent before rolling up into turbulent eddies.

More precisely, the TrSL is divided by Zdravkovich (1997) in three stages: the lower-, intermediate- and upper-subcritical regime. The typical flow structures of the TrSL state are the so-called transition eddies.

At first, undulations of both free shear layers develop from the separation lines in TrSL1. They are called Gerrard-Bloor transition waves and were first described by Gerrard (1978). Such waves are symmetric on the two sides of the cylinder and in-phase, therefore they are not related to the alternating eddy shedding. Zdravkovich (1997) describes an analogy between the onset of instability and oscillation of the

laminar Karman-Bénard street (L3) and the onset of these undulations in the free-shear layers (TrSL1).

In TrSL2, the transition eddies appear before transition to turbulence. They were firstly sketched by Couregelongue (1929) during outdoor experiments in a river and appeared as "chains" of small eddies along the free shear layers. As Re increseas, there is a progressive movement of transition towards separation and it is accompanied by a shortening of the eddy formation region (L_f), so that the eddies are brought closer to the base of the cylinder. A reduction in L_f is always reflected in a decrease in $C_{p,b}$ (higher suction in the wake, thus higher drag) and an increase in C'_L (higher lift fluctuations), because the eddies form closer to the body. However, the S_t number does not change significantly from TrSL1 (elongation of the formation region) to TrSL2 (shortening of the formation region). Because of that, Gerrard (1966) suggested that the shedding frequency is primarily related to the distance between the two free shear layers, which varies through TrSL but not so largely as the variation of L_f. In particular, according to Gerrard (1966) and Bloor and Gerrard (1966), two opposite tendencies seem to cancel each other in order to keep the same strength of the turbulent eddies in TrSL2, thus an almost constant S_t: the shortening of the formation region and the widening of the turbulent shear layers. In addition, in the TrSL2 regime the shortening of L_f counteracts the increase in the shear layer thickness, since thick turbulent shear layers need more time for a roll up to be carried across the wake.

As the shortening of the eddy formation region is completed, at the end of TrSL2, the transition eddies disappear and TrSL3 begins. It is characterized by a wide near-wake (small angle of separation), high suction in the wake, high drag and high lift fluctuations due to the very short length of the formation region L_f. Zdravkovich (1997) describes the transition to turbulence as a sudden burst in the free shear layers close to the cylinder. Three-dimensional flow structures develop in the near-wake, responsible for a significant reduction of the correlation length along the span. The interesting feature of TrSL3 is the stabilizing effect produced on the transition in the free shear layers in this range of Re, so that the upper subcritical regime is defined as a quasi-invariable flow. The reason is that the wide near-wake (produced by short L_f) displaces the free shear layers into the free stream and causes the acceleration of the stream adjacent to the near-wake. This has a stabilizing effect, so that the transition region does not progress upstream with increasing Re. As a consequence, TrSL3 is characterized by almost constant $C_{p,b}$, C_D (the horizontal stretch before the critical fall in the drag), C'_D and C'_L (see Figure 3.3) and S_t number as well.

Transition in the boundary layer

The stabilizing effect, which characterizes the quasi-invariable nature of the flow in the subcritical range - due to the accelerated free stream that squeezes the separated shear layers that surround the wide wake - gradually weakens with rising Re, as the free-shear layers become more aligned with the adjacent free stream. Transition to turbulence advances in the free shear layers towards separation until it reaches the separation line. It starts then a complex interaction between transition and separation, which was first observed by Taylor (1916) and better investigated by Fage in 1928. Zdravkovich (1997) names this regime transition in the boundary layer TrBL (Re from 10^5-$2*10^5$ – according to Zdravkovich, but generally somewhat arbitrary in literature – to an undefined upper limit, in the order of 10^6, which marks the entering in fully turbulent conditions).

The beginning of TrBL is marked, according to Zdravkovich, by the initial fall of the drag coefficient (Re = 10^5-$2*10^5$), due to a reward movement of the separation point. Instead, according to Schewe, 1983 the key feature which denotes such a boundary between subcritical and critical regimes is the onset of randomization of lift fluctuations, at a slightly higher Re (in Schewe's results, Re = $2.8*10^5$ marked the onset of random lift fluctuation, while Re = $1.4*10^5$ was at the initial fall of the drag).

This initial stage (TrBL0), which Zdravkovich includes in the critical regime, is named pre-critical. The decrease in the drag coefficient is the result of the narrowing of the wake and a gradual displacement of separation downstream with rising Re (Achenbach&Heinecke, 1981). The length of the eddy formation region L_f, which was short in TrSL3, elongates and the roll up of the free shear layers is displaced downstream. This reduces the negative base pressure and weakens the alternate pressure fluctuations on the two sides of the cylinder. The small suction in the wake is associated to high maximum lateral suction and this is the reason for the fall in the drag coefficient and the rise of the pressure recovery. Bearman (1969) noticed that the S_t number remains constant in TrBL0. Again, the constancy of S_t is related to two opposite tendencies: on one hand the free shear layers tends to get closer, but the elongation of L_f leads to a slight widening.

The state TrBL1 is named by Zdravkovich single bubble regime, followed by TrBL2 that is the two-bubble regime.

Eisner (1925) was the first who measured stable asymmetric mean pressure distributions around a circular cylinder in a certain range of Re. He concluded, correctly, that transition occurred on one side only of the cylinder. Only at slightly higher Re, transition could complete on the two sides. When this happens, C_D reaches

the minimum value (at Re = Re_{cr}). However, the state of flow in this particular range of Re was deeply investigated only several years later (Achenbach, 1968; Bearman, 1969; Farell and Blessmann, 1983; Schewe, 1983). The key feature is the formation of laminar separation bubbles, either on one side only or on two sides of the cylinder.

The formation of laminar separation bubbles on two sides of a cylinder (at Re ≈ Re_{cr}) was identified by Achenbach (1968) through measurements of skin friction. He found that at Re = 10^5, at ϕ = 105° (ϕ = 255°) there was not a final separation. In fact, there was a region between laminar separation and turbulent reattachment in which the wall shear stresses theoretically vanished. Downstream, there was an intensive rise of the skin friction, showing that the boundary layer was turbulent. Turbulent separation occurred finally at ϕ = 147° (ϕ = 220°).

In 1969, Bearman identified a bistability of the flow in a sub-range of Re before symmetric twin bubbles appeared by experimental evidence of discontinuous changes in $C_{p,b}$ and S_t at Re = $3.4*10^5$ and $3.8*10^5$. He found the cause in the formation of a laminar separation bubble on one side only of the cylinder. The $C_{p,b}$ distribution along the height showed that the bubble took place along the complete length of the cylinder. He also noted that the asymmetric pressure distribution was accompanied by the displacement of the stagnation point away from the bubble.

Further studies on the formation of only one bubble are reported by Farell and Blessmann (1983). Contrary to the results of Bearman (1969), who found the single-bubble regime to occur always with the bubble consistently on the same side of the cylinder, in Farell and Blessmann's experiments no preference was detected for the bubble to form on either side of the cylinder.

Schewe (1983) described in detail the physical phenomenon of a laminar separation bubble on one side only of the cylinder. A discontinuity in the drag coefficient and a sudden jump of S_t (up to 0.33) mark the onset of a bistable flow condition (Figure 3.1, letter c). The name explains that there are two stable states, corresponding to the two possible signs of the lift force. The asymmetric stable state persists for a very small range of Re. Then, a second discontinuity in the drag, as well as another sudden jump in S_t (up to 0.48 that is the highest value, letter f in Figure 3.1) marks the abrupt disappearance of the steady lift and the attainment of the minimum drag, corresponding to the critical Re. The bistable flow condition is preceded and followed by two unstable ranges (corresponding to S_t = 0.2 and 0.31 respectively, according to Figure 3.4). Such unstable ranges correspond to the letters a, b and d, e in Figure 3.1.

"The explanation for the phenomena", Schewe writes, "lies in the behaviour of the boundary layer. The asymmetric flow and thus the steady lift in the critical range is

caused by the fact that the boundary layer transition from laminar to turbulent has occurred on one side only of the cylinder. Thus a laminar separation bubble is formed as follows: the transition from laminar to turbulent flow occurs in the detached boundary layer just downstream from the separation point. After reattachment of the boundary layer on the back of the cylinder, the separation is turbulent." Figure 3.2 shows the asymmetry of laminar and turbulent separations on the two sides of the cylinder. Figure 3.6 reports a clear representation made by Basu (1985) of the flow field near the point of separation in transitional range of Re, with formation of a laminar separation bubble.

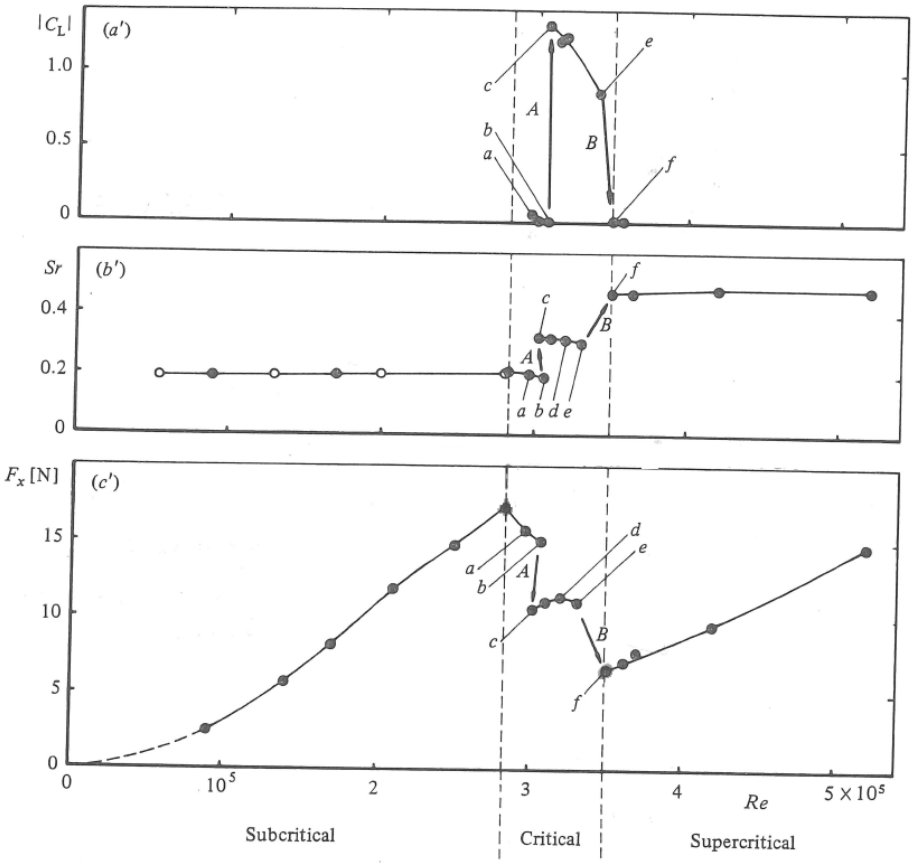

Figure 3.1 Steady lift, Strouhal number and drag force. Asymmetric bistable flow indicated by letter c (Schewe, 1983)

The reason for which transition in the detached boundary layer is initiated on one side only of the cylinder and not simultaneously on both sides is the occurrence on that side of perturbations or fluctuations, which are inherent in the boundary layer and in the free stream. Then, once transition and then reattachment have occurred on one side, there is an acceleration of the fluid on that side and deceleration on the other side. Since deceleration delays transition in the free shear layer (it reduces Re), the formation of the bubble also on the other side is delayed. According to Schewe (1983) this is the reason which stabilizes and fixes the asymmetric flow state. Of course, such

a bistable flow condition is extremely sensitive to Re and is possible only if there is a very low probability for simultaneous occurrence of perturbation on both sides. In fact, the bistable flow disappears on rough cylinders as well as in turbulent flow.

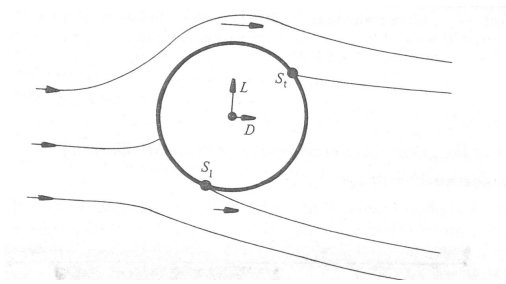

Figure 3.2 Asymmetric flow state in the critical regime of Re (Schewe, 1983)

As soon as the flow also reattaches on the other side of the cylinder, symmetric conditions are again achieved with two bubbles on the two sides of the cylinder: the drag is then minimum and that is the critical Re. Zdravkovich defines this symmetric state of the flow as two-bubble regime (TrBL2) and it precedes the supercritical (TrBL3) regime. The latter begins with the fragmentation and disruption of bubbles and it is characterized by large scatter of results and suppression of vortex shedding, due to high three-dimensionality of the flow. Slightly different in the nomenclature and in the subdivision of the flow regime, is the classification proposed by Roshko (1961) and Achenbach (1971): the supercritical regime starts immediately after the critical drop and for the smooth cylinder it is at first stable, with two separation bubbles and narrow band lift fluctuations, i.e. regular vortex shedding. According to this classification, vortex shedding is rather evident in the first stage of supercritical flow, with the highest Strouhal value (S_t = 0.48 according to Schewe, 1983). Then, the upper transition range is an unstable state, characterized by suppression of vortex shedding, which marks the transition to the transcritical regime.

Until the surprising discovery made by Roshko in 1961, it was believed that once the boundary layer becomes turbulent upstream of the separation the periodic eddy shedding should cease due to the irregular and chaotic state of the free shear layers. Instead, Roshko discovered that the periodic eddy shedding reappears in what he called transcritical regime. That is, referring to Zdravkovich's nomenclature, TrBL4 or post-critical regime. In this regime, all the C_D curves by different authors show the same trend: they rise up to a certain Re in the TrBL3 and level out in the TrBL4 regime. It means that the separation point is essentially fixed. According to Achenbach's classification, the more or less constant position of the separation point is

the boundary between what he defined supercritical and transcritical regimes, at about Re = $5*10^6$.

3.2.3 Fully turbulent state

Above TrBL4, Zdravkovich concludes the classification with the fully turbulent state (T). Theoretically, it is reached when all the three disturbed regions (wake, free shear and boundary layers) are fully turbulent, i.e. transition is very close to stagnation. In practice, it is not defined, in terms of Re, neither the beginning of T (i.e. the end of TrBL4) nor the end. Transition should reach the stagnation point when Re → ∞, so that the final regime is called ultimate. However, compressibility effects in air appear at high Re and they become the governing parameters. Anyway, what is accepted for sure, is that (Roshko, 1961) "it seems unlikely that there will be any further transitions once all disturbed regions around the cylinder are turbulent". The invariance of the flow pattern implies that all coefficients remain constant as Re increases.

3.2.4 Summary

Figure 3.3 (Zdravkovich, 1990) summarizes the behaviour of the mean drag and rms value of the lift coefficients for the whole range of Re.

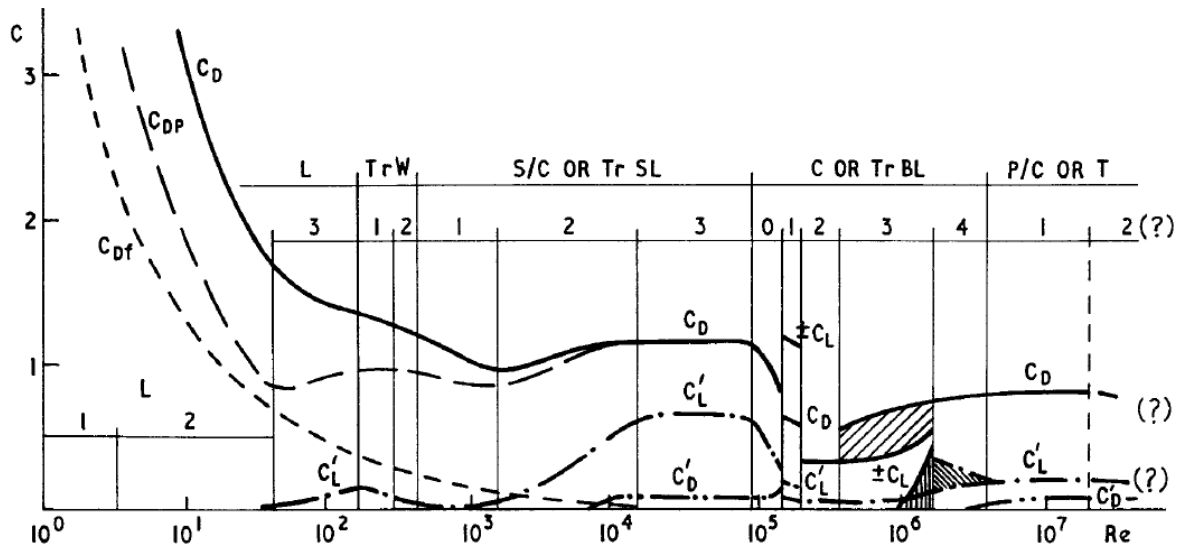

FIG. 2 Force Coefficients versus Reynolds Number; C_D - mean drag, C_{Df} - friction drag, C_{DP} - pressure drag, C_D^1 - fluctuating drag, C_L - mean lift C_L^1 - fluctuating lift.

Figure 3.3 Force coefficients versus Reynolds number (Zdravkovich, 1990)

Relying on Schewe (1983)'s results and in accordance with Roshko and Achenbach's classification of the regimes of flow, Niemann&Hölscher (1990) suggest, for the smooth cylinder, the following review (Figure 3.8):

				discontinuity A, hysteretic		discontinuity B, hysteretic	upper transition	
	(1)	(2)	(3)	(4)	(5)	(6)	(7)	(8)
state of boundary layer	stable		unstable	bistable	unstable	stable	unstable	stable
10^5 Re	1,4	2,8	3,0	3,3	3,5	10	50	
mean drag c_D	1,2	1,2 - 1,0	1,0 - 0,7	0,5	0,5 - 0,4	0,22	0,22 - 0,52	0,52
mean lift c_L	0			± 1,3	1,3 - 0,9	0	0,1 ... 0,2	0
fluctuating lift: SDF	single narrow peak		random with two peaks	narrow peak	random + peak	narrow peak	random, two broad peaks	rather narrow peak
Sr	0,2		0,2	0,33	0,31	0,48	(0,1/0,45)	0,28
$c_{L,rms}$	0,4 - 0,25	0,25 - 0,09	0,09 - 0,06	0,04	0,04 - 0,07	0,02	0,04	0,05
boundary layer and separation	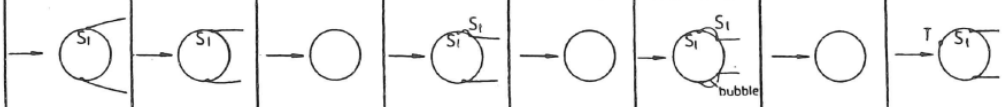							
	laminar separation S_l	laminar separation	random changes	one-sided separation bubble	random changes	two-sided separation bubble	random changes	turbulent separation S_t

Figure 3.4 Smooth circular cylinder – review (Niemann&Hölscher, 1990)

The flow field near the point of separation in different Re regimes is well depicted by Basu (1985). It is reported in Figure 3.5 (at subcritical Re), in Figure 3.6 (in the transitional range, with formation of a laminar separation bubble) and in Figure 3.7 (at transcritical Re).

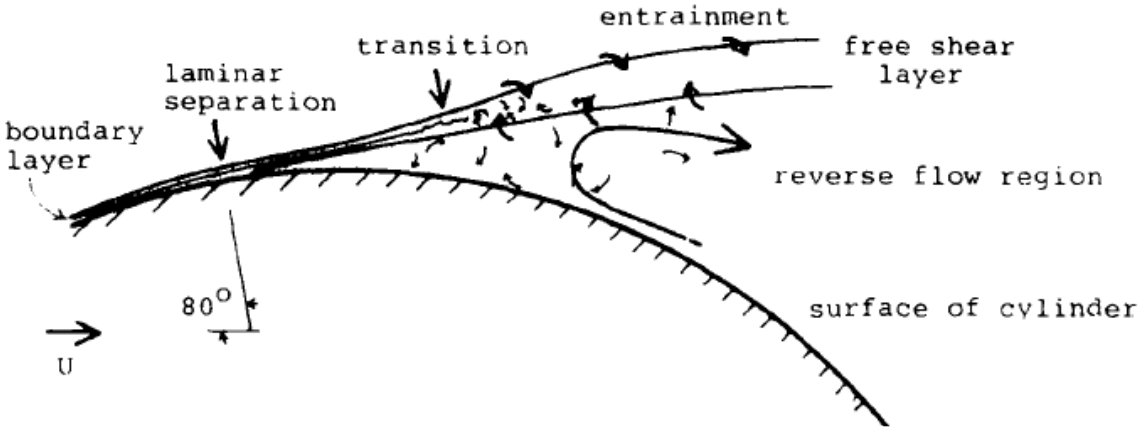

Figure 3.5 The flow field near the point of separation: subcritical Re (Basu, 1985)

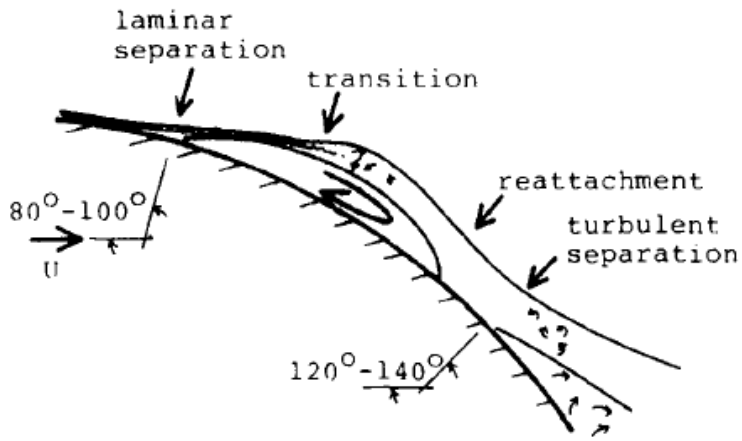

Figure 3.6 The flow field near the point of separation: transitional Re (Basu, 1985)

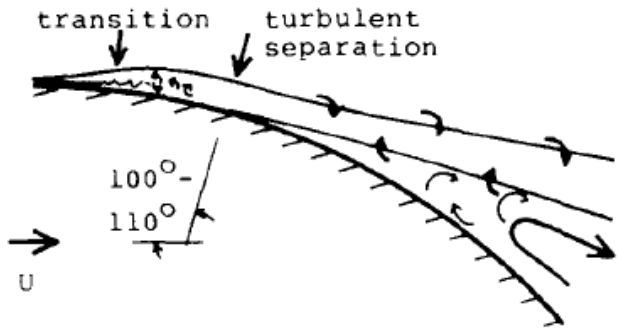

Figure 3.7 The flow field near the point of separation: transcritical Re (Basu, 1985)

3.3 Effect of surface roughness

The flow pattern around a circular cylinder is primarily determined by the position of the separation point. Such a location is governed by the Reynolds number and strongly influenced by the roughness of the cylinder surface and to some extent also by the turbulence characteristics of the approaching flow. Surface roughness is often used in wind tunnel tests as a simulation technique of high Reynolds numbers.

A practical approach to quantify this effect is proposed in the ESDU 74030 and results in the calculation of the so-called effective Reynolds number (Re_e). This is a modified Re, which incorporates a factor λ_R depending on surface roughness, and a factor λ_T depending on incoming turbulence. Re_e reproduces, at lower Reynolds numbers, the same effects in the flow that would occur at higher Reynolds numbers. It is then a useful tool in wind tunnel tests on scale models.

$$\mathrm{Re}_e = \mathrm{Re}\,\lambda_R \lambda_T \tag{3.2}$$

Increasing surface roughness and/or turbulence of the incoming flow has the effect of increasing the boundary layer thickness and enhancing transition from laminar to turbulent flow, so that transition occurs at progressively lower Re. This explains the decrease in the critical Re. In addition, increasing surface roughness increases the value of C_D at Re_{cr}, while increasing incoming turbulence does not change the value of C_D at Re_{cr} significantly. The effect of incoming turbulence will be addressed in the next section, while this section addresses the effect of surface roughness. Surface roughness is especially effective in triggering transition in TrBL and the effectiveness depends on the height of roughness elements with respect to the thickness of the boundary layer. Pioneering experiments on the effect of surface roughness were carried out by Fage and Warsap (1929). They showed that the steep drop in the steady drag occurs at progressively smaller Reynolds numbers with increasing surface roughness.

Milestone studies on the influence of surface roughness on circular cylinders at high Re (up to $3*10^6$), obtained in atmospheric and high-pressure wind tunnel, have been published by Achenbach (1971) and Achenbach&Heinecke (1981). Similarly to what Roshko (1961) proposes for a smooth cylinder, the curve representing the drag coefficient as a function of Reynolds number for a rough cylinder (Achenbach, 1971) is divided into four parts (Figure 3.8). Each range – subcritical, critical, supercritical, transcritical, respectively – is characterized by a special boundary layer behaviour. According to Achenbach, "the subcritical flow regime is not yet influenced by the surface roughness. In a large range of Reynolds number the drag coefficient is nearly constant. Increasing the Reynolds number the drag coefficient suddenly drops. This range, the lower limit of which is dependent upon the roughness conditions, is denoted the critical flow regime. Exceeding the Reynolds number of minimum C_D the drag coefficient grows up again (supercritical range) and reaches a nearly constant value in the transcritical range. This transcritical drag coefficient increases with rising roughness parameter".

Achenbach studied the behaviour of the boundary layer by measuring local pressures and skin friction. In subcritical flow regime the boundary layer separates laminarly. At immediately higher Re, the disturbances produced by surface roughness "support the boundary layer with energy from outside". Thus, the boundary layer can remain adjacent to the wall over a larger distance. The separation point shifts to the back of the cylinder and this reduces the drag coefficient, although the separation is still laminar (critical range). At minimum C_D, laminar separation and turbulent reattachment occur. This is the phenomenon of the separation bubbles, as previously

described on smooth cylinders. However, it is remarkable that this phenomenon – clearly visible in the horizontal plateau at $C_{D,min}$ for smooth cylinders (Figure 3.9) – is restricted to a very narrow flow range if the surface of the cylinder is rough. In fact, as proved by Buresti (1981) and stated in the review by Niemann&Hoelscher (1990), the extension of the critical and supercritical range is diminished on a rough cylinder. The critical range basically consists in a shift downstream of separation (without the unstable and bistable flow ranges observed on smooth cylinders) and then the drag increases to its transcritical value due to an upstream shift of the transition point. Moreover, as previously said, with increasing roughness the minimum of C_D at the critical Reynolds number increases.

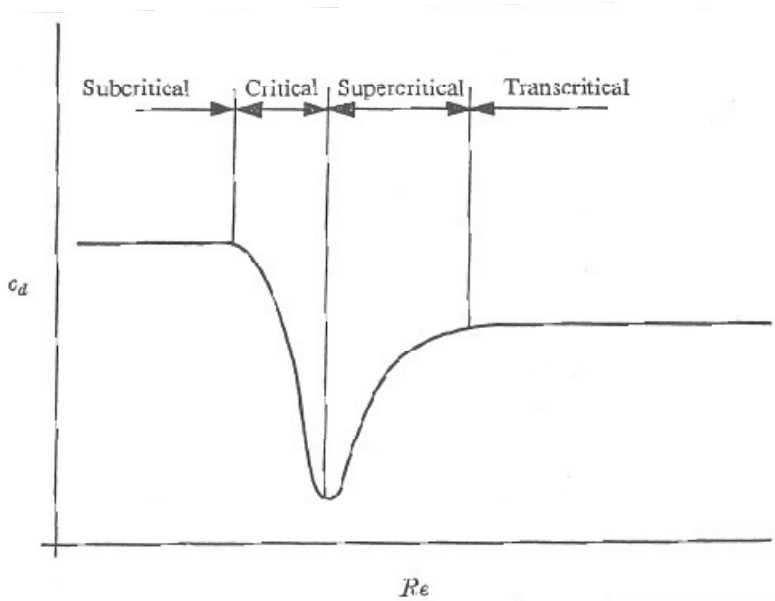

Figure 3.8 Definition of four ranges for the flow past a rough circular cylinder (Achenbach, 1971)

Figure 3.9 reports the different behaviour of the Strouhal-versus-Re curve on a rough cylinder. In particular, on a rough cylinder the Strouhal number exhibits an increase in the critical flow regime, but with growing roughness parameter the step in the curve becomes smaller (Achenbach&Heinecke, 1981). In any case, this is much smaller than the constant value of the Strouhal number due to the formation of laminar separation bubbles on a smooth cylinder (range 6 in Figure 3.9). The smaller S_t and the higher $C_{D,min}$ at critical Re on a rough cylinder, with respect to a smooth cylinder, are due to the upstream shift of the location of boundary layer separation. In other words, higher roughness produces earlier separation. This is confirmed by Achenbach (1971): "with increasing roughness parameter, the angle of separation becomes smaller (≈110°) compared with that of the smooth cylinder (≈140°) at critical flow conditions".

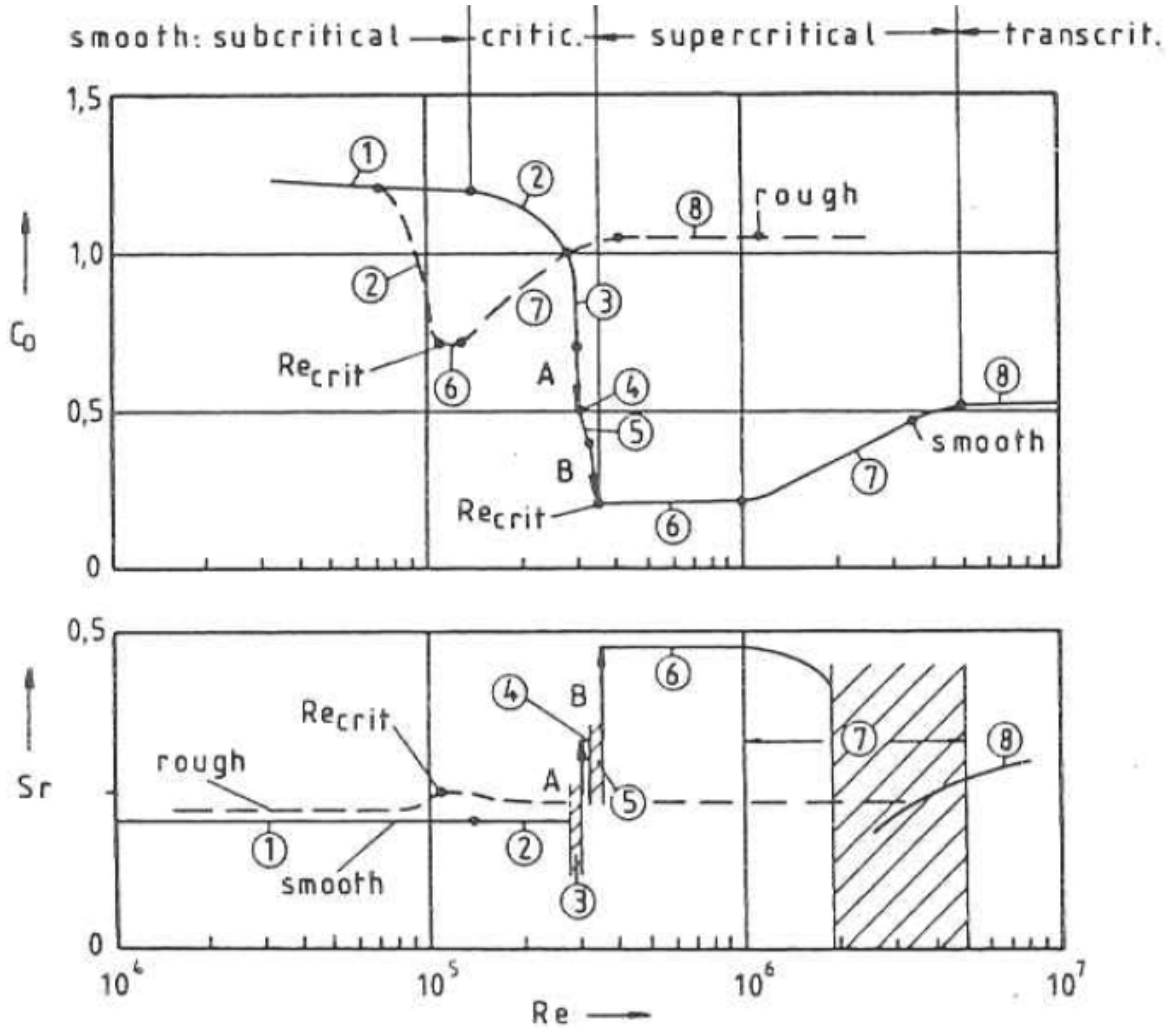

Figure 3.9 Flow regimes for smooth and rough cylinders. The corresponding flow regime description is counted in Figure 3.4 – review (Niemann&Hölscher, 1990)

Various surface roughness types are investigated by Achenbach&Heinecke (1981). Despite the differences in the curves (in terms, for example, of C_D and S_t), the fundamental boundary layer phenomena are the same for all roughness types. However, "the boundaries between the various regimes, as well the supercritical and post-critical drag coefficients and Strouhal numbers are a function of both the size and the type of surface roughness" (Buresti, 1981). In the same years, Güven et al. (1980) measures the effects on the mean flow past circular cylinders due to five different sizes of distributed sandpaper roughness. In particular, the pressure rise to separation results to be closely related to the characteristics of the boundary layer; smaller pressure rise is associated to thicker boundary layers. Larger roughness gives rise to a thicker and more retarded boundary layer which separates earlier and with a smaller pressure recovery. The influence of meridional ribs on the development of the boundary layer around a circular cylinder is calculated by an analytical method in Güven et al. (1983). Ribeiro (1991) investigates "which types of surface roughness are more efficient in

triggering a transition of the flow so as to simulate the mean and fluctuating pressures occurring at ultra-critical Reynolds numbers". Among sand paper, wire mesh screen and ribs, he finds that "all the roughness types were efficient in triggering regime transitions and in allowing the establishment of the ultra-critical regime with relatively low Reynolds numbers". However, "an increase in relative roughness progressively distorts the mean pressure distribution results (distorts in the sense of deviating from what is observed with smooth circular cylinders)". Therefore, he suggests that "the smallest relative roughness to establish ultracritical conditions should be chosen for simulation problems of cylindrical structures with circular cross-section and smooth surface". Moreover, Ribeiro also observed that "the mean values of the force and pressure coefficients obtained with the ribs model were closer than any of the others to the values observed on smooth circular cylinders. The behaviour was such that, with regard to mean values, the rib roughness type seems the most appropriate to be employed in simulation problems of cylindrical structures of circular cross-section and smooth surface, because of its efficiency in establishing the ultra-critical condition and because it does not interfere excessively with the mean force and pressure coefficients". According to Ribeiro, the same conclusion regarding the use of ribs also holds regarding the fluctuating loads, although the fluctuating values measured on the rough circular cylinders (at relatively low Re values) were larger than those observed on the smooth cylinder at high Re values.
Other important contributors on the topic are for example Batham (1973), who measured pressure distributions on smooth and rough cylinders at critical Reynolds numbers in uniform and turbulent flows; Szechenyi (1974, 1975), who performed supercritical Reynolds number simulations for two-dimensional flow over circular cylinders; Nakamura&Tomonari (1982), who studied the effect of different types of surface roughness at high Reynolds numbers; Basu (1985), who gathered data from a large number of experiments in order to describe the behaviour of the mean drag coefficient, the Strouhal number and the rms lift coefficient as functions of Re and relative roughness. In recent years, the effect of surface roughness on lift forces has been investigated by Eaddy (2004).

Last but not least, the effect of surface roughness is not only a simulation technique of high Reynolds numbers, but it is utilized for example on cooling towers to reduce wind-induced stresses in shell structures, by reduction of high lateral peaks of suction (VGB, 2010). However, this is not the case of solar towers, which should be smooth in full-scale in order to be subjected to lower drag forces (Figure 3.10b).

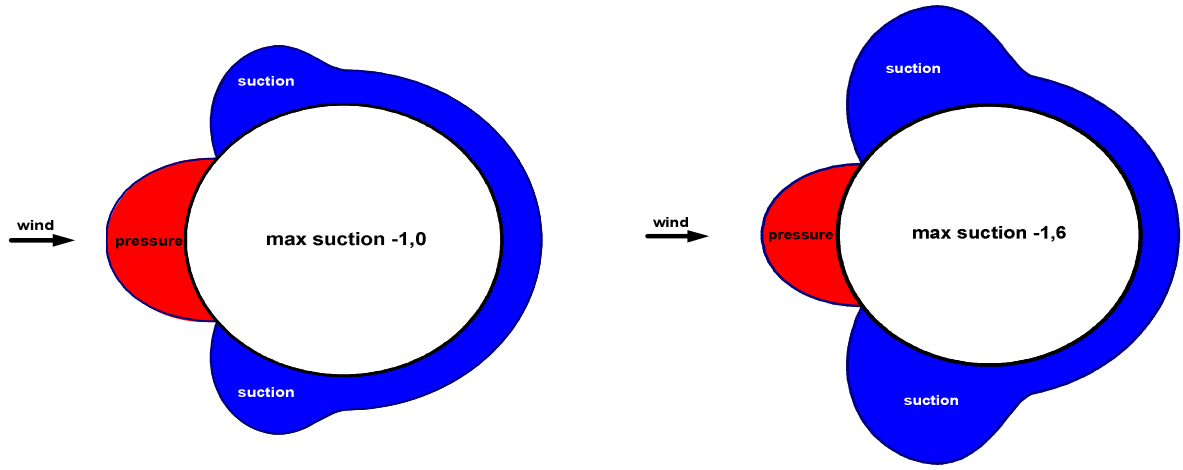

a) *b)*

Figure 3.10 Mean pressure distribution at transcritical Re
a) rough surface, $C_{D,m}$ = 0.66; b) smooth surface, $C_{D,m}$ = 0.46 (Niemann, 2009).

3.4 Effect of free-stream turbulence

Free stream turbulence is basically characterized by two parameters: the turbulence intensity σ_U/U_m and the integral length scale of the longitudinal component L_{ux}. For very large ratios L_{ux}/D, longitudinal velocity fluctuations are perceived as slow changes in the mean wind speed and lateral fluctuations as slow changes in wind speed direction. Under these conditions, the quasi-steady approximation can be used to evaluate pressure fluctuations, by applying equation (3.3) (Basu, 1986). Instead, when L_{ux}/D ratios are small, further complication arises because turbulence is distorted by the presence of the body.

$$Cp_{\sigma}(\varphi)=\left\{\left[\left(\frac{2\sigma_u}{U_m}\right)Cp_m(\varphi)\right]^2+\left(\frac{dCp_m(\varphi)}{d\varphi}\right)\left(\frac{\sigma_v}{U_m}\right)^2\right\}^{1/2} \tag{3.3}$$

Incoming turbulence modifies mean pressures and forces on a circular cylinder because it induces earlier transition to turbulence in the cylinder boundary layers or in the separated shear layers than would occur in smooth flow. Since small-scale turbulence is better able to interact with the cylinder boundary layers and shear layers than large-scale turbulence, at large turbulence scale-to-diameter ratios the interaction between free-stream turbulence and the cylinder boundary layers and wake is reduced, so that premature transitions are less likely to occur (Basu, 1986). Moreover,

depending on the intensity of turbulence, two mechanisms play a major role: at low levels of turbulence the main effect is to disrupt the coherence of vortex shedding; at higher levels of turbulence the enhanced entrainment from the near wake into the shear layers dominates. Because of this last mechanism, while the influence of incoming turbulence on the fluctuating pressures in the stagnation region is direct, in the wake region it is more subtle. In fact, the wake region is separated from the external flow by the presence of the free-shear layers and only at sufficiently high intensity the small-scale turbulence is able to penetrate. Since the principal influence of free-stream turbulence is in the stagnation region, while the influence on the wake is quite weak, it is often assumed that the pressure fluctuations at the rear of the cylinder are independent on the incident turbulence.

As previously mentioned, further complication arises from the distortion that the turbulence experiences as the flow approaches and passes the cylinder. Hunt (1972) developed a theory, namely rapid distortion theory, to predict the modification of turbulence near a structure, and how these changes depend on the shape of the structure and on the scale of the turbulence relative to the structure. Once the disturbed flow field near the structure is mathematically described, the pressure fluctuations on the body surface can be predicted. This is the core of the theory, which aims to identify the effects of the incident turbulent on the unsteady velocities near a bluff body invested by wind and on the fluctuating pressures on its surface.

The effects of the incident turbulence should be distinguished from the effects of the self-induced unsteady velocities and surface pressures, which are induced near a structure when a completely steady wind blows around it. They are due to separated flows at the sides and rear of the obstacle and to instability of the flow at the ground or at the tip. The theory assumes that the intensity of the upwind turbulence is weak and it does not interact with the velocity fluctuations induced by the wake. In this way, the velocity fluctuations outside the wake caused by eddies shed at the wake boundaries are statistically independent on the velocity fluctuations caused by the upwind turbulence. Therefore, the two types of velocity fluctuations can be analyzed separately (Hunt, 1975). This assumption is only approximately true. In fact, fluctuations of the incident wind can strongly effect the fluctuations caused by eddy shedding. For example, if there is a significant amount of energy in the velocity fluctuations of the incident wind at frequencies close to the eddy shedding in the wake, the eddy shedding may be amplified. Experiments by Britter et al. (1979) showed that the vortex shedding peak is altered by the incident turbulence, because it may occur at a slightly lower frequency and be more broad. In general, problems to the applicability

of the theory arise if there is an appreciable correlation between wake induced fluctuations and velocity fluctuations in the incident turbulence. The correlation results from the modification of the self-induced fluctuation due to incoming turbulence. However, this should not be significant if $\sigma_{u,\infty} << U_{m,\infty}$, i.e. the turbulence of the incoming (undisturbed) flow is weak. Moreover, it is interesting to note that the addition of a splitter plate, which is able to suppress vortex shedding, improves the agreement between the theory and the experiments.

The core of the theory – which allows to consider the self-induced velocity fluctuations in the external region (resulting by the unsteady wake) as statistically independent on the velocity fluctuations produced by upwind turbulence – is the rapid distortion of turbulence by changes in the mean velocity produced by the body. In other words, turbulence is disturbed so rapidly by changes in the mean velocities close to the body, that each wave number (or eddy) is distorted separately before it can exchange energy non-linearly with other wave numbers. Therefore, a limitation of the theory is that it is linear. In fact, non-linear effects can be important, especially at high frequencies, where non-linear terms do not decay as rapidly as the linear terms. In any case, a good applicability of the theory is guaranteed if the time scale for the non-linear interaction between energy-containing eddies (L_{ux}/σ_u) is large compared with the time required for the fluid to flow round the obstacle (a/U_m where "a" is used in Figure 3.11 to indicate the cylinder radius). In other words, if $(\sigma_u/U_m)(a/L_{ux}) << 1$, then the turbulence is primarily distorted by the mean velocity field before it can be modified significantly by non-linear interactions: the distortion is rapid. This criterion for linearization – suggested by Hunt (1973) – is considered even too restrictive in Durbin&Hunt (1980) and re-formulated in that paper.

The changes in the turbulent velocity field in the disturbed region near the structure have a simple physical explanation. Two phenomena explain qualitatively the amplification or reduction of the turbulent components: [1)] distortion by the mean flow of the turbulent vorticity; [2)] blocking or source effect caused by turbulence impinging on the cylinder surface. Near the stagnation point the vortex lines in the x-direction are decreased while those in the y-direction are stretched and those in the z-direction are unaffected (two dimensional case, far from end conditions). So, at stagnation, the eddies which are small compared to the structure are piled up and stretched out. Instead, if the turbulence scale is much larger than the radius of the cylinder there is no effect of vortex stretching, only a blocking effect of the cylinder (Hunt, 1975).

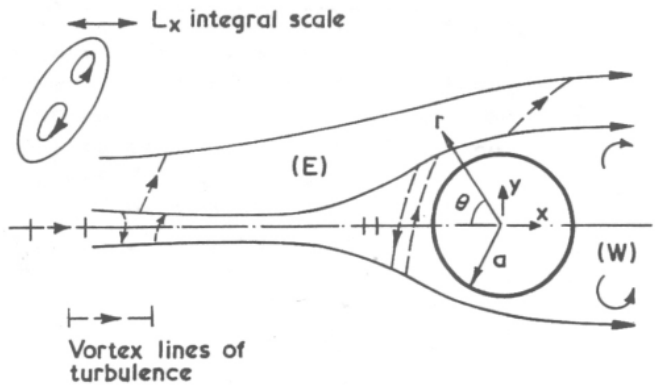

Figure 3.11 Mean streamlines around a circular cylinder showing compression and stretching of vortex lines (E stands for external region, W stands for wake region) (Hunt, 1975)

By assuming a rapid distortion, the movement of vortex elements can be described by the movement of line elements (Figure 3.11) and the movement of line elements is known if the mean velocity field near the body is known. The field of mean velocity will stretch and rotate vortex lines, altering the distribution of turbulent vorticity and thus changing the turbulent velocities. This stretching and rotating of vortex lines will take place over a distance in which the mean velocity field is significantly altered by the bluff body, i.e. over a distance a few times the radius of the cylinder (Britter et al., 1979). Instead, the blocking effect produces a change in the turbulence over a distance comparable to the scale of turbulence L_{ux} or the cylinder radius a, whichever is smaller. The relative importance of the distortion effect over the blocking one increases as a/L_{ux} increases or the distance from the cylinder increases. The effect of turbulence scale with respect to the diameter of the cylinder is demonstrated in (Hunt, 1973) by measuring the ratio between the rms values of the u-components in the undisturbed flow and in the disturbed flow near the structure ($\sigma_{u,\infty}/\sigma_u$) as a function of the ratio between cylinder radius and L_{ux} (a/L_{ux}). The issue is further addressed in Britter et al. (1979). Figure 3.12 (Britter et al., 1979) summarizes these results. If turbulent eddies are small with respect to the cylinder diameter (small scales, $a/L_{ux} >> 1$), on the stagnation line σ_u increases and σ_v decreases. However, close to the surface where both vorticity distortion and the source effect are significant, the amplification of σ_u decreases and σ_v increases. For large scales ($a/L_{ux} << 1$) the source effect dominates, turbulence is blocked by the cylinder and consequently σ_u decreases and σ_v increases. At the flanges of the cylinder (90°) the opposite occurs. The vortex lines of small scale eddies are stretched in the x-direction, but reduced in the y-direction, so that σ_u is reduced (x-direction) and σ_v is increased (y-direction), while the blocking effect acts in the cross-wind direction.

Hunt's theory predicts results for the two asymptotic limits $L_{ux}/a >> 1$ and $L_{ux}/a << 1$. The large scale limit is described by the well-known quasi-steady theory (equation (3.3)), while the small-scale limit is introduced by Hunt as a quasi-homogeneous or slowly varying approximation, where the turbulence vorticity around the body is given in terms of the upwind fluctuating vorticity and the mean velocity field. The latter is given by the standard potential-flow solution for a circular cylinder, as if separation does not take place. The quasi-steady theory for large scales is simpler than the small scale theory, because the incident vorticity is not distorted by the obstacle, which only blocks the flow. For intermediate scales, it is not practical to apply the rapid distortion theory, but reasonable extrapolation formulas (e.g. for the stagnation point) are proposed in Durbin&Hunt, 1980. In any case, whatever the value of L_{ux}/a, if the frequency is sufficiently high the results for spectra tend to the limiting situation where $L_{ux}/a << 1$.

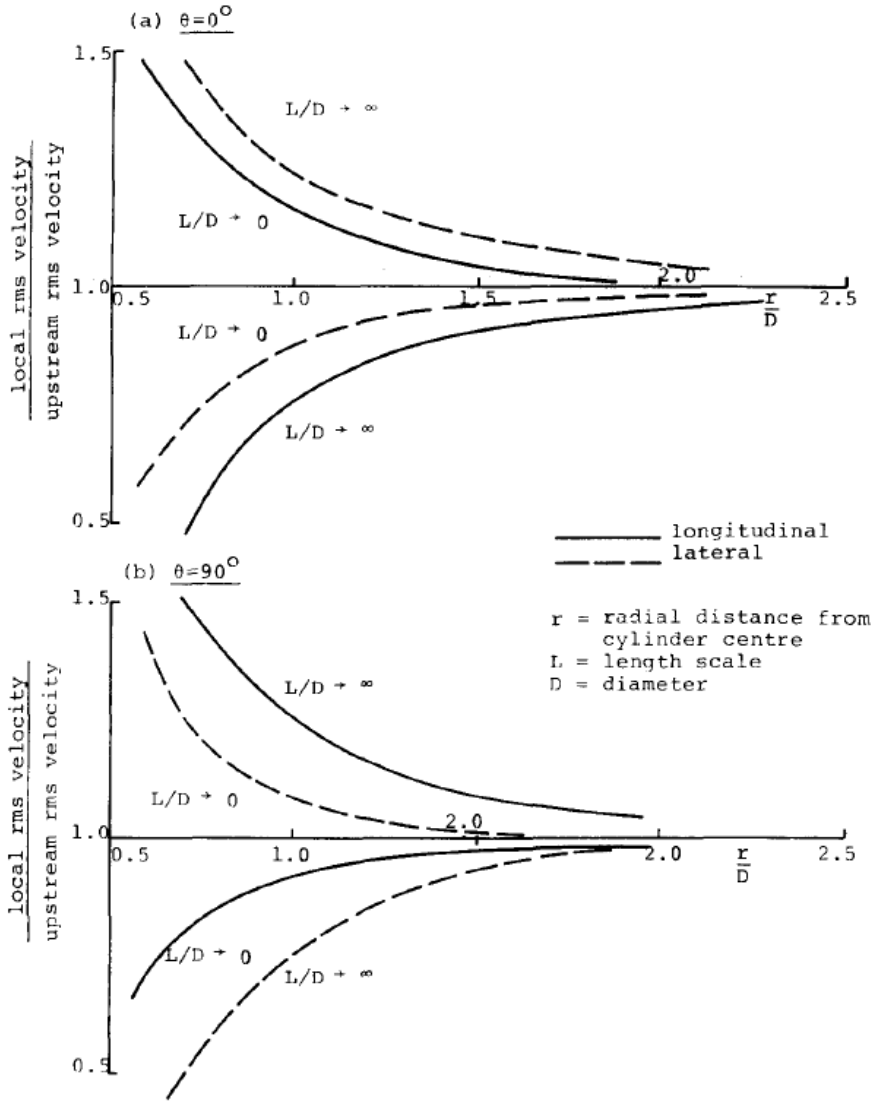

Figure 3.12 Modification of fluctuating velocities near the cylinder in small- and large-scale turbulence (Britter et al., 1979)

This Dissertation does not go further into the mathematical model behind Hunt's theory (Hunt, 1972, 1973). However, the physical principles represented the basis to develop the wind load model in Chapter 7. Such physical principles have been applied to experimental data measured in two wind tunnels (WiSt and CRIACIV) in order to separate turbulence-induced and body-induced pressure fluctuations (section 7.1.3).

3.5 Three dimensional effects

This section addresses the aerodynamic of the flow around finite-length circular cylinders of high aspect ratio, characterized by Karman vortex shedding, where end-effects still dominate for large part of the height. Solar updraft towers are represented at best by this category. Three dimensional effects arise at the top due to the free end and at the bottom due to the ground surface. They depend on the aspect ratio, on the boundary layer conditions (uniform or shear layer) and on Re. Literature at high Re is scarce, therefore most of the experiments and simulations mentioned in the following are performed in sub-critical conditions.

In the ground-wall region, a three dimensional separation of the boundary layer occurs upstream of an obstacle and a so-called horseshoe (or necklace) vortex system develops at the base of the body. In fact, the cylinder end is submerged in a retarded wall boundary layer and an adverse pressure gradient is created. This causes the three dimensional boundary layer separation at some distance upstream of the body, followed by a roll-up of the separated boundary layers into a system of swirls. The swirl system is swept around the base of the cylinder and assumes a characteristic shape, which is responsible for the name "horseshoe vortex".

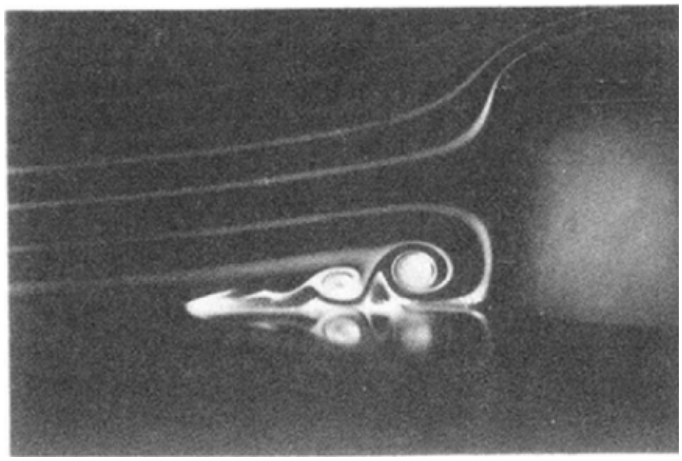

Figure 3.13 Horseshoe vortex system: experiment by Sutton (1960) in laminar boundary layer, reported in Baker (1991)

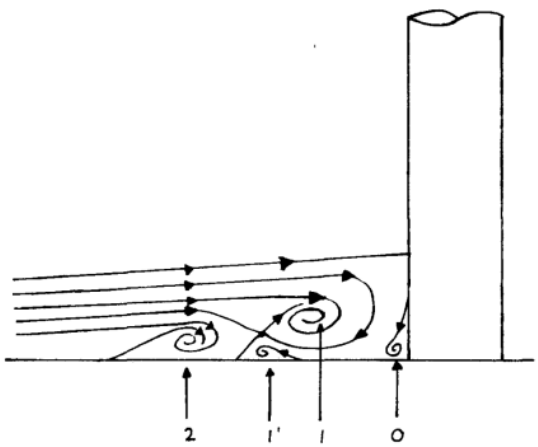

Figure 3.14 Turbulent horseshoe vortex system: sketch by Baker (1980)

As explained by Zdravkovich (2003), the physical parameters governing the horseshoe vortex system and the number of swirls are the thickness of the wall boundary layer and the cylinder diameter. The wall boundary layer may be laminar or turbulent, depending on the Re of the boundary layer, which includes the flow velocity and viscosity and – as characteristic length – the thickness of the boundary layer. If the upstream boundary layer on the wall is laminar, then the flow pattern results in steady laminar horseshoe vortices, as those shown in Figure 3.13. This is an early photograph taken by Sutton (1960) and reported in Baker (1991). There are three clockwise and three anticlockwise rotating vortices on the plane of symmetry upstream of the cylinder.

A literature review about laminar and turbulent vortex systems is presented in Baker, (1978, 1980). In particular, Figure 3.14 (Baker, 1980) shows the flow pattern of a turbulent horseshoe vortex upstream of a cylinder at low Re ($4*10^3 < Re < 9*10^4$). Four vortices (0, 1, 1' and 2) are detected in the figure. Vortex 1 is the main or primary vortex, vortex 1' is caused by separation of the boundary layer beneath vortex 1. Vortex 0 is caused by separation of the boundary layer on the upstream face of the cylinder. Baker (1990) studies the oscillatory behavior of horseshoe vortices in the transitional regime, between the steady laminar horseshoe vortices which occur at low Reynolds number and the fully turbulent horseshoe vortices that occur at higher Reynolds numbers.

The distance from the boundary layer separation to the cylinder depends on the height and diameter of the cylinder. When the height is greater than the wall boundary layer thickness, the separation is independent on the height of the cylinder. According to Belik (1973), such a distance lies between 0.45D and 0.65D. Baker (1991) also measured that for H/D > 1 the separation length tends to 1.1D, independent on H/D.

The size of the horseshoe vortices, relative to the height of the cylinder, decreases as the height of the cylinder increases (Okamoto&Sunabashiri, 1992). Zdravkovich (2003) estimates that the mean pressure distribution along the cylinder, at the cylinder foot, is modified by the horseshoe vortex system for a spanwise distance of about only one third of the diameter.

Hölscher (1993) measured the pressure distribution on the ground plane around a finite circular cylinder of low aspect ratio (H/D = 2). Roughly, the circumferential pressure on the cylinder surface is reflected on the ground plate. Positive pressures on the windward surface of the cylinder also act on the ground plate in the region upwind of the body. This study indicates that the extension is about one diameter upwind of the

junction for a body totally immersed in a turbulent boundary layer. It is directly correlated to the size of the horseshoe vortex system. As the surface pressures on the cylinder decrease with the circumference, negative pressures arise on the ground plate. However, maximum suction appears in the near wake in the plane of symmetry and not at the side of the cylinder. The unsteadiness of the wake flow generates significant pressure fluctuations. They even exceed the pressure fluctuations on the windward side, which are on the other hand directly determined by the turbulence intensity of the approaching flow. Due to the free-end effect, the base pressure in the wake of a short cylinder is higher than in the case of a tall cylinder. Taniguchi (1981) and Okamoto&Sunabashiri (1992) provide comparisons of surface pressure distribution on the ground plane for cylinders of different aspect ratios.

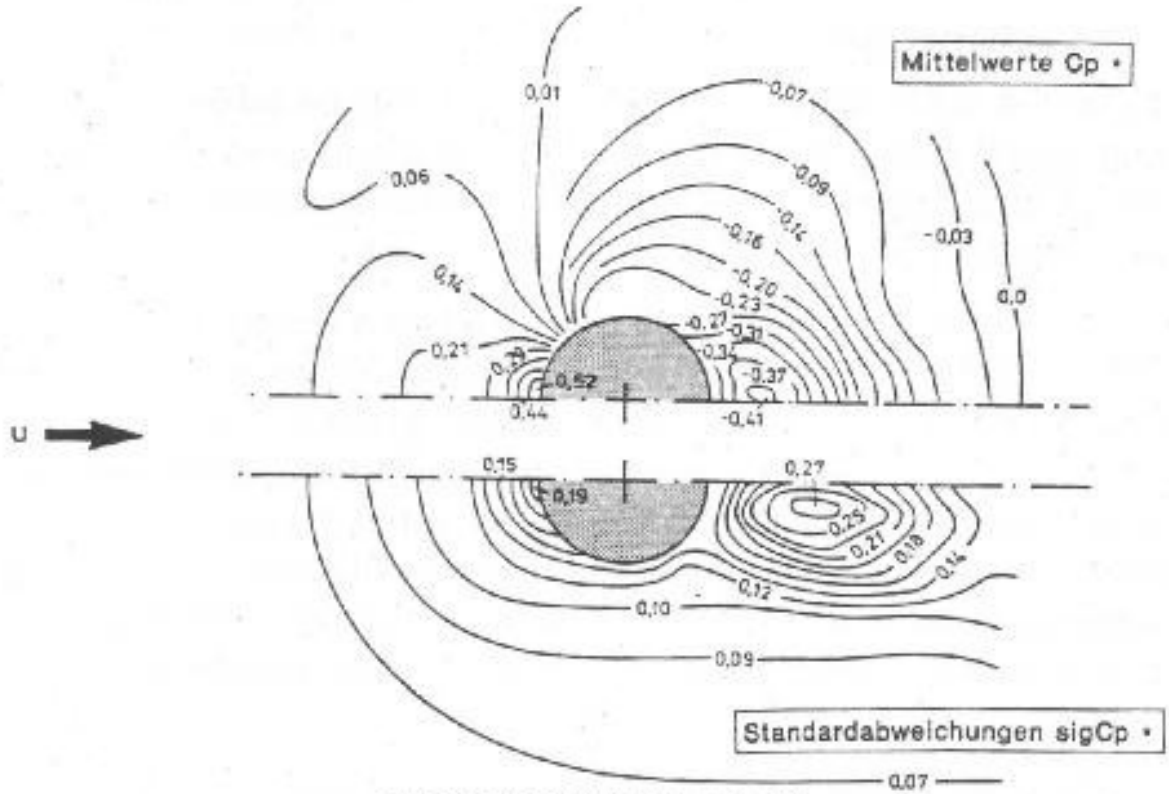

*Figure 3.15 Pressure distribution on the ground plane around a finite circular cylinder. Top: mean pressure coefficient, bottom: rms-value of pressure fluctuations. H/D = 2, Re = 3.1*10^5 (Hölscher, 1993)*

In the wake, the surface pressures on the ground plane are the result of a time-averaged recirculation region behind the cylinder and depend on the aspect ratio. For small aspect ratios, the streamlines over the top of the cylinder reattach to the ground plane downstream. Okamoto&Sunabashiri (1992) identified the size of such a recirculation region for cylinders of different aspect ratio. Tests were performed in uniform flow at

Re = 2.5-4.7*10^4. According to those results, the recirculation region enlarges with an increase in H/D, as long as H/D ≤ 4. But the recirculation region decreases in the case H/D ≥ 7, because the end effect is limited to the portion near the free-end. The steady recirculation region observed in the experiments by Palau-Salvador et al. (2010) on a H/D = 5 circular cylinder at Re = 2.2*10^4 is instead somewhat smaller (Figure 3.17).

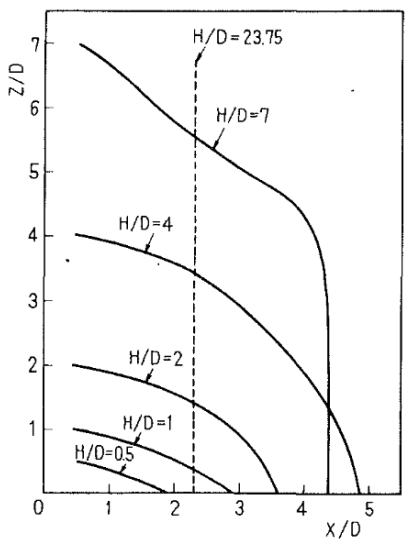

*Figure 3.16 Wake recirculation, Re= 2.5-4.7*10^4 (Okamoto&Sunabashiri, 1992)*

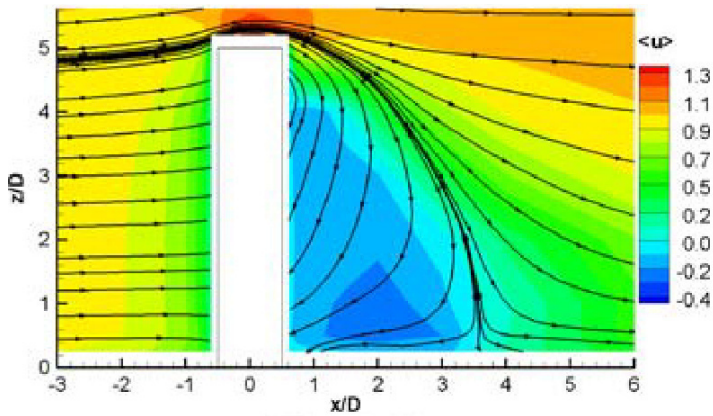

*Figure 3.17 Recirculation region in the wake, H/D = 5, Re = 2.2*10^4 (Palau-Salvador et al., 2010)*

A recent investigation on the influence of the aspect ratio on the wake structure is presented in Rostamy et al. (2012) and summarized in Figure 3.18. The study, based on a PIV visualization, is performed in flat-plate turbulent boundary layer on cylinders of aspect ratio H/D = 9, 7, 5, 3 and at Re = 4.2*10^4. The cylinders have a close end. The study highlights the strong downwash in the near-wake region, which originates near the free-end and descends in the central portion of the wake. The large recirculation zone is marked by the "dividing streamline"; the flow above it moves away from the cylinder. Within the recirculation zone, a small vortex forms immediately below the free-end. The size of this vortex varies with the aspect ratio; the largest vortex occurs for the smallest aspect ratio (H/D = 3). Depending on the size of this vortex, the flow in the tip region can move upwards along the cylinder wall toward the free-end, as it happens in Figure 3.18 c and d (H/D = 5 and 3, respectively). Near the ground, a weak upwash flow can be seen for H/D > 3, which moves towards the central region of the wake. This creates a vortex, namely base vortex, near the cylinder wall-junction. For H/D = 3 the base vortex and the upwash are absent. This is not surprising, because the wake structure of a low aspect ratio circular cylinder is completely different (for example symmetric arch-type vortices develop), as it will be

explained in the following. For all the aspect ratios, a saddle point (black point in the figure) is identified between the two vortices near the free-end and near the cylinder-wall junction. This point marks the streamwise extension of the recirculation zone, as previously identified by Okamoto&Sunabashiri (1992). Accordingly, the saddle point moves downstream as H/D increases, below H/D = 7 up to x/D = 3.8. Results are not too far from Palau-Salvador et al. (2010). For H/D = 9 the saddle point moves closer to the cylinder at x/D = 3.

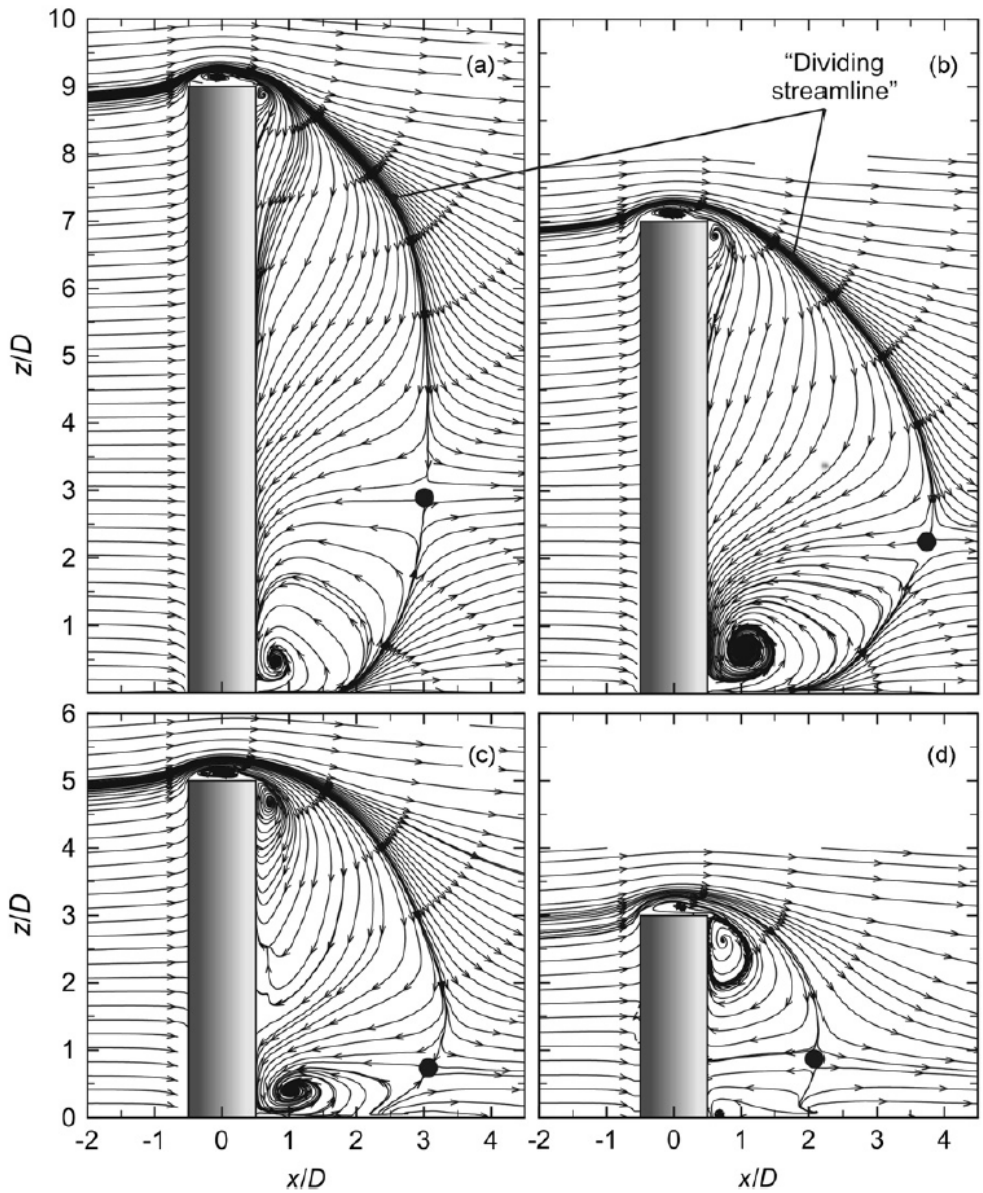

*Figure 3.18 Mean streamline field in a vertical plane on the wake centreline for: a) H/D = 9; b) H/D = 7; c) H/D = 5; d) H/D = 3; Re = 4.2*10^4, flat-plate turbulent boundary layer (Rostamy et al., 2012)*

A clear visualization of the near-wake flow behind a H/D = 6 circular cylinder at Re = 2*10^4 is described by using LES in Krajnovic (2011). Particular attention is paid to the upwash flow and the base vortices in uniform flow, namely N_w in the paper (with left

and right legs N_{wl} and N_{wr}). "As seen in Figure 3.19, the flow in the symmetry plane moves towards the cylinder near the ground and bends down after the stagnation point, forming the N_w vortex. While the lower part of the near wake is dominated by the downwash very close to the cylinder, the upwash dominates further downstream. This is a result of the two legs, N_{wl} and N_{wr}, rotating in counter-clockwise and clockwise directions, respectively (Figure 3.19 high right-hand side corner)". In the symmetry plane downstream of vortex N_w (Figure 3.19 low right-hand side corner), a focus F_{nw} and a saddle point S_{nw} are visible. They indicate the closure of the separation region in the near wake".

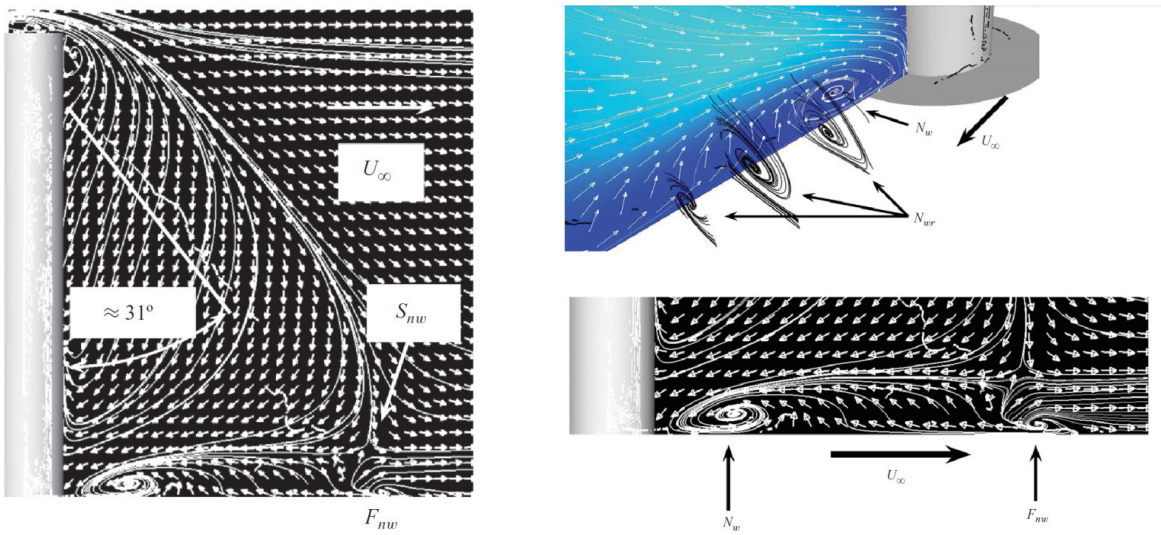

*Figure 3.19 Near wake visualized with vortex cores, streamlines and velocity vectors H/D = 6, Re = 2*10^4, uniform flow (Krajnovic, 2011)*

An analogous simulation, but in boundary layer flow (Sumner&Heseltine, 2008, H/D = 3 to 9, Re = 6*10^4) showed a similar base vortex pair (distinct from the horseshoe vortex) close to the ground. However, probably due to the boundary layer, the vortices are of different size and at higher position if compared to those in Figure 3.19. Figure 3.20 shows the strong downwash behind the cylinder and the weak upwash near the ground plane, which is associated to the base vortices. It is confirmed in this paper, that for low aspect ratios (e.g. H/D = 3) the downwash extends almost to the wall, while the base vortices and so the upwash are absent: the wake structure is then completely different. A further proof is observed by using PIV in Rostamy et al. (2012).

A flow visualization of the surface flow pattern at the base of a circular cylinder at high Re is also published by Gould et al. (1968) and shown in Figure 3.21. It refers to uniform flow conditions, but a certain boundary layer is naturally developed at the tunnel floor. The figure clearly shows the downstream movement of the separation line

at the ground. The importance of these experiments, is that they are performed on a smooth cylinder in a pressurized wind tunnel up to Re = $5.4*10^6$. Therefore, they represent one of the few tests available in literature in transcritical conditions. Because of that, they will be often used as reference in the following.

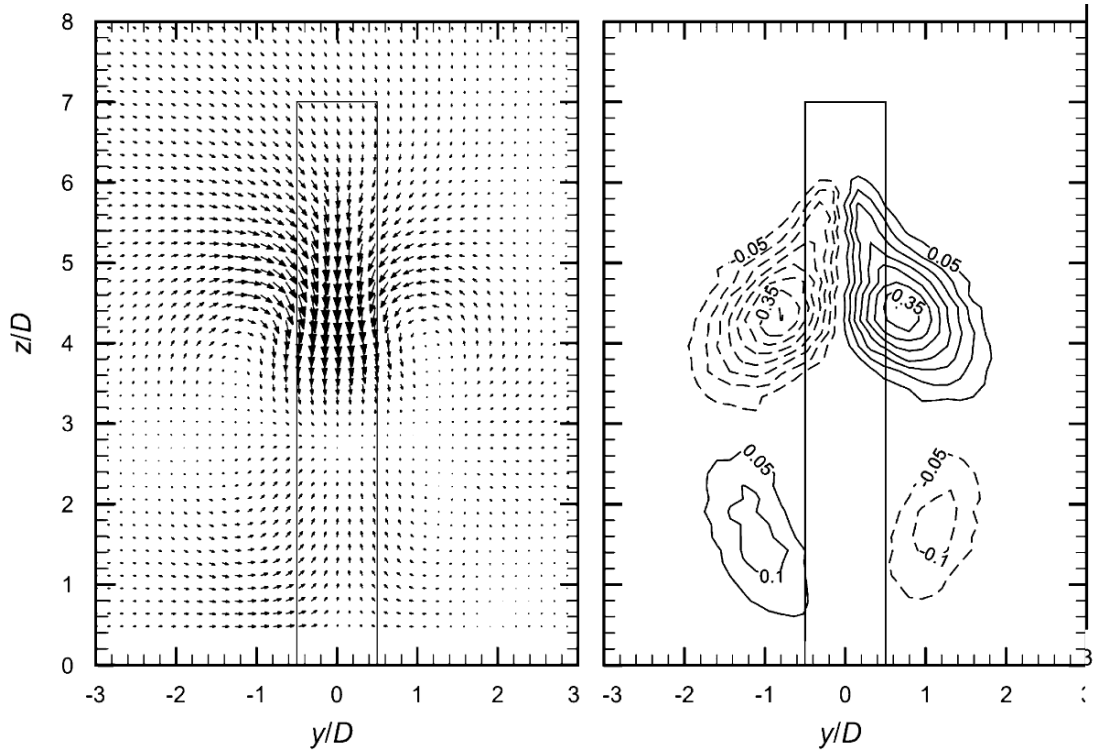

Figure 3.20 Time-averaged wake structure: in-plane velocity field and streamwise vorticity field behind the cylinder (dimensionless vorticity contour increment 0.05, minimum vorticity contour ±0.05, solid line represent counter clockwise vorticity, dashed lines represent clockwise vorticity). H/D = 7, Re = $6*10^4$, boundary layer flow (Sumner&Heseltine, 2008)

In the tip region (Figure 3.22), because the pressure induced by the flow on the forward facing surface is significantly higher than that on the rearward facing surface, a flow is induced over the tip of the cylinder from front to rear. The separated flow over the tip creates a region of very low pressure, which induces a spanwise flow towards the tip of the cylinder. This flow sweeps up the separated shear layers from intermediate heights. At short distance below the free-end (about D/2), vortex sheets roll up into a pair of trailing (tip) vortices, which form because of the interaction between the upward-directed separated flow at the sides of the cylinder and the downward-directed flow over the tip. The tip vortices are counter-rotating open vortex loops with their axis perpendicular to both the free-stream direction and the longitudinal axis of the cylinder. The tip effect is governed by the difference of pressure between the front and the rear surfaces of the cylinder and it extends for the upper two or three diameters. In sub-critical flow conditions the wake suction is high

(thus high drag), therefore it is expected that the tip effect in sub-critical conditions is more vigorous than in transcritical conditions, being the latter accompanied by a smaller wake with a lower base suction (ESDU 96030).

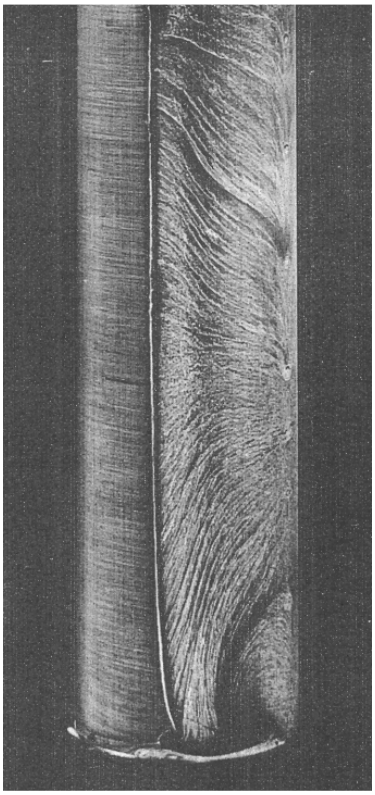

Figure 3.21 Flow pattern in the bottom region at high Re (Gould et al., 1968)

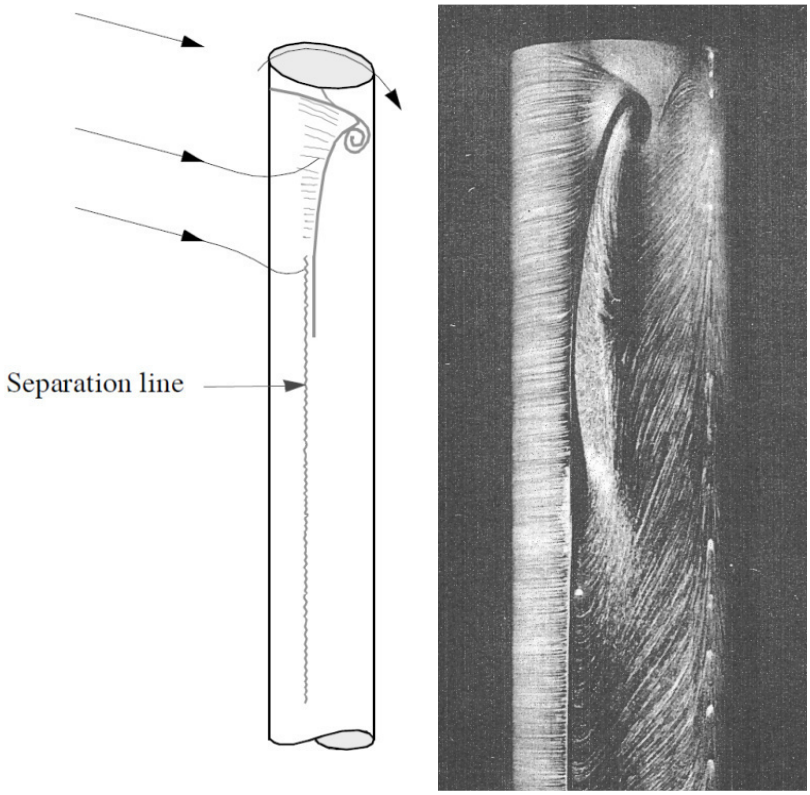

Figure 3.22 Flow pattern in the tip region:
a) Sketch of tip trailing vortices (ESDU 96030);
b) Flow visualization at high Re (Gould et al., 1968);

In presence of an efflux from a chimney, wind tunnel tests show that, at sub-critical Reynolds numbers (Re < 10^5), the effect of the efflux is to increase the response. However, at higher Reynolds number (as it is for solar towers) the effect is likely to be reversed (ESDU 96030).

Gould et el. (1968) also investigated the effect of efflux. In their experiments without efflux, it is confirmed the presence of tip vortices originating from the top of tower, within the plane where the local drag coefficient is maximum (i.e. at D/3 from the top, where D stands for diameter), as shown in Figure 3.22. In presence of efflux, it is noticed that there is a distortion of such a pattern. As a result, the vortices can be seen at one diameter from the top (instead of D/3). Gould et al. suggested that the effluent plume generates another pair of vortices just above the top of the chimney. These are opposite in sign to the original pair present in the absence of efflux. As the velocity of the efflux increases, the upper pair of vortices increases in strength and causes a displacement and weakening of the original pair. The apparent effect of an efflux is

thus to raise the height at which the peak loading is experienced to a level closer to the top of the chimney. In such a way, there is an extension of the quasi-two dimensional region (out of the influence of the tip effect), where the drag and lift coefficients are smaller. Moreover, it is also observed in practice that if a chimney is seen to oscillate, then increasing the efflux by opening the flues will generally reduce the oscillation amplitude. Thus, at high Reynolds numbers, it is likely to be conservative to assume that the no-efflux condition presents the more critical design case (for both the along and the across wind response). The ESDU Data Items (ESDU 81017) give the same recommendation. In particular, when H/D is greater than 4 the drag coefficient is larger when the free-end is not closed, but if there is an efflux from the open end the drag coefficient is reduced approximately to the value it would have with a closed end. It is then common practice (at least for what concerns the mean load) to design a stack with the top open and no-efflux.

In summary, the three-dimensional flow pattern around a slender finite length circular cylinder, is characterized by the horseshoe vortices forming upstream at the cylinder-wall junction, a recirculation region in the near-wake, with a small vortex below the free-end and base vortices near the ground plate. The latter develop strongly in boundary layer flows as a result of an upwash near the ground. In the tip region, there are counter rotating open vortex loops, named tip vortices. As regards the fluctuating field, there is the familiar Karman vortex shedding from the sides of the cylinder. This may present, along the height, a variation of the Strouhal number, as it will be explained afterwards. Now, the mean and rms loading pattern on the cylinder surface is analyzed.

In literature, one of the first studies of the spanwise distribution of mean force and pressure coefficients in uniform and shear flow for different aspect ratios has been carried out by Okamoto and Yagita (1973, 1984) at Re = $1.3*10^4$. The mean iso-pressures lines for a slender circular cylinder (H/D = 9) in uniform flow and shear flow (uniform shear flow) are reported inFigure 3.23 and Figure 3.24, respectively. The velocity profile for the uniform shear flow of those experiments has a non-dimensional velocity gradient of 0.4 and it is expressed by the relation: U(z)/U(H/2) = 1 + 0.4*(z/H – 1/2).

Figure 3.23 and Figure 3.24 show that the free-end effect is limited to the upper three diameters and it is not affected by the boundary layer conditions. Only for smaller

aspect ratios (H/D ≤ 5 according to Okamoto&Yagita, 1984) the end effect would reach the root of the cylinder.

A typical feature of the mean surface pressure distribution in the tip region is the minimum pressure around $\phi \approx 70°$ at z' ≈ 2/3D from the free-end. It is due to the displacement of the separation to higher angles. Then, a second islet of minimum pressure appears at $\phi \approx 135°$ and z'/D ≈ 1/3 from the free-end. This second $C_{p,min}$ arises considerably the local drag near the free-end. In fact, the $C_{D,max}$ is more pronounced on slender cylinders (H/D ≥ 7) and it is followed by a decrease at lower levels. $C_{D,max}$ exceeds the value of the nominal drag for two-dimensional circular cylinders (Figure 3.27 and Figure 3.28)

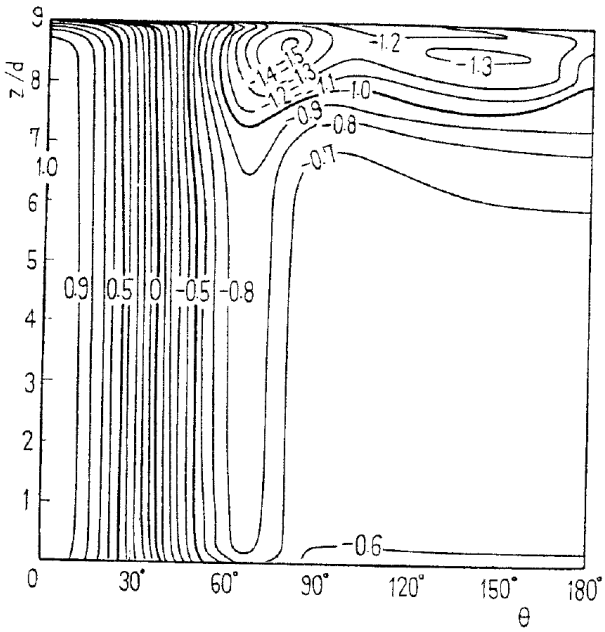

*Figure 3.23 $C_{p,m}$ in uniform flow. H/D = 9, Re = 1.3*10^4 (Okamoto&Yagita, 1984)*

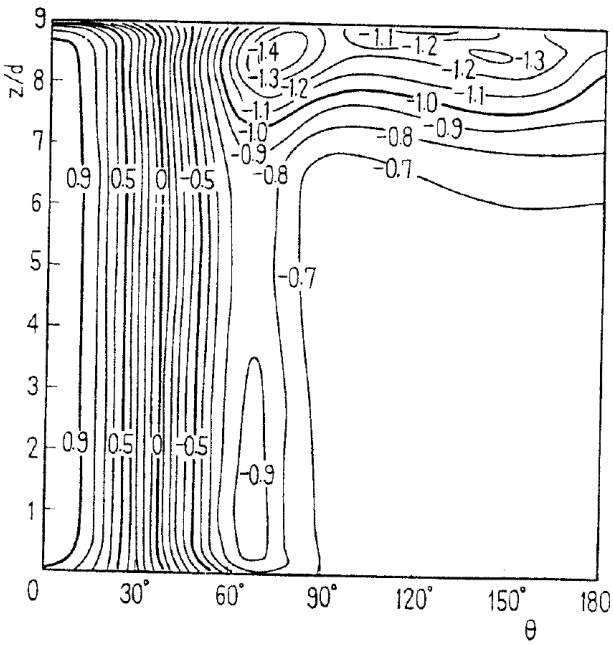

*Figure 3.24 $C_{p,m}$ in uniform shear flow. H/D = 9, Re = 1.3*10^4 (Okamoto&Yagita, 1984)*

The bottom region of the cylinder in figure Figure 3.24 is influenced by the shear flow condition, but the effect is not so strong. In the low region, at the stagnation line, the C_p distribution tends to deviate from the unitary value due to the downflow produced by the horseshoe vortices. This effect is enhanced by the velocity gradient in shear flow. In shear flow there is also an increase in lateral suction at the base of the cylinder. It has, however, little effect on the drag, which results to be uniform along the height below the tip region for H/D = 9, both in uniform and in shear flow (Figure 3.27 and Figure 3.28).

At higher aspect ratios, e.g. H/D = 12, and in shear flow, the region of low pressures at the rear side gradually extends towards the root of the cylinder (Figure 3.25). The increase in wake suction at the bottom (see Figure 3.26 at high aspect ratios) implies

higher drag in the low region of the cylinder. It is remarkable that this occurs for sufficiently high aspect ratios and only in shear flow, as confirmed by Figure 3.28.

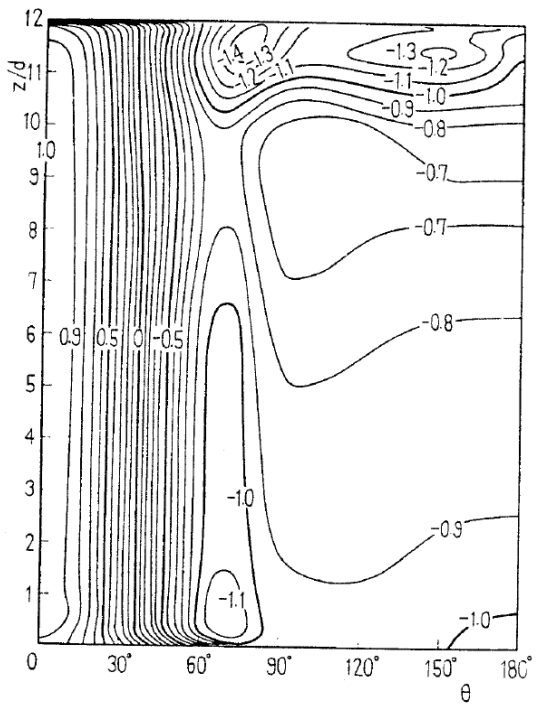

*Figure 3.25 $C_{p,m}$ in uniform shear flow. H/D = 12, Re = 1.3*10^4 (Okamoto&Yagita, 1984)*

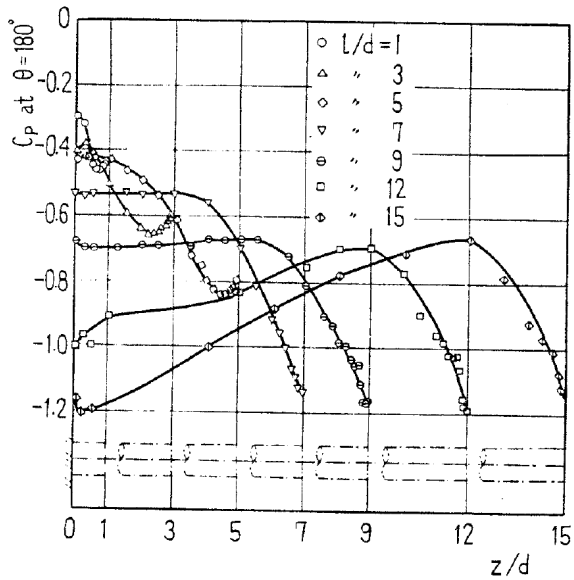

*Figure 3.26 $C_{p,m}(180°)$ in uniform shear flow. H/D from 1 to 15, Re=1.3*10^4 (Okamoto&Yagita, 1984)*

It is remarkable to further comment the comparison of local drag coefficients in uniform and shear flows in Figure 3.27 and Figure 3.28: the mean drag at low levels is constant in uniform flow, while it rises in shear flow when the aspect ratio is sufficiently high. The authors mention the existence of a secondary flow in the rear of the cylinder, which does not appear in the uniform stream. They conclude that "the pressure at the rear side of the cylinder of H/D ≥ 12 gradually decreases and the local drag coefficient increases as the root of the cylinder in a uniform shear stream is approached, while the pressure at the rear side of the cylinder of H/D ≥ 7 is nearly constant in the lower portion free from the end effect in a uniform stream".

With this regard, Farivar (1981) confirmed that in uniform flow (Re = 7*10^4) the base pressure coefficient is independent on height in the range 0.39 ≤ z/H ≤ 0.81. At z/H ≤ 0.39 the variation of the base pressure was attributed to the boundary layer at the tunnel floor. Luo et al., 1996 showed that in uniform flow (at Re = 3.33*10^4) the pressure in the stagnation region is relatively insensitive to variation of both H/D and spanwise location, with exception near the free-end. Instead, the pressure in the wake shows strong aspect ratio and spanwise position dependence. This is mainly due to tip

effects, while the spanwise dependence is greatly reduced at z/H ≤ 0.5. This is in agreement with other results in uniform flow.

In boundary layer flows, Garg&Niemann (1995) observed that on a smooth cylinder of H/D = 8.5 at Re = $6.7*10^4$, the spanwise mean drag distribution is comparable to the ones in Figure 3.28, characterized by increasing values at the top (due to the tip effect) and also the bottom. The results in this Dissertation (Chapter 4) confirm this trend on a rough cylinder in atmospheric boundary layer, although this peculiar distribution is ignored in many Codes (e.g. Eurocodes).

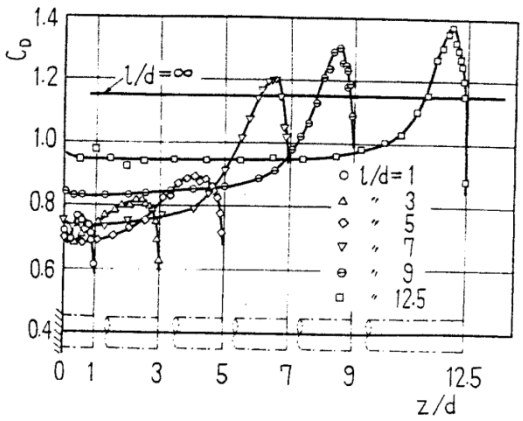

Figure 3.27 Local drag coeff. $C_{D,m}$ in uniform flow, Re=$1.3*10^4$ (Okamoto&Yagita, 1984)

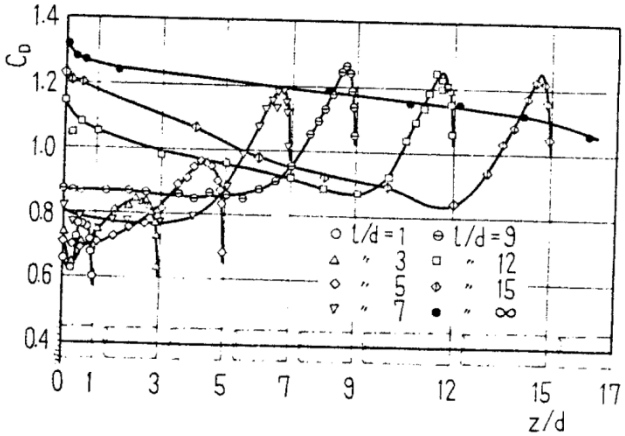

Figure 3.28 Local drag coeff. $C_{D,m}$ in uniform shear flow, Re=$1.3*10^4$. (Okamoto&Yagita, 1984)

The non-uniformity of the drag coefficient along the height of the cylinder below the tip region (i.e. apart from tip effects) in boundary layer flow – which primarily depends on higher suction in the near wake at low levels – can also find an explanation by looking at Figure 3.19 compared to Figure 3.20 (Krajnovic, 2011 and Sumner&Heseltine, 2008, respectively): the position of the base vortex pair in the time-averaged wake structure rises significantly in boundary layer flow. On low aspect ratio cylinder (H/D < 3), instead, base vortices are absent.

Consistently with what has been said about the non-uniformity of the mean drag in the low region in boundary layer flows, the ESDU Data Items (ESDU 81017) suggest to apply – in boundary layer flows – a correction factor, which allows to calculate the value of the local mean drag coefficient in the specific boundary layer flow condition by amplifying the C_D value in uniform flow. The extent and the magnitude of the correction depend on the local shear flow gradient.

The reason provided by the ESDU for such a correction factor, namely f_{sz}, is that in boundary layer flows stronger spanwise velocity gradients enhance the flow movement

from regions of relatively high pressure to regions of relatively low pressure. This produces higher local drag coefficients at the base of the structure. In particular – as explained by the ESDU – on the front face of the cylinder in boundary layers flow the pressure decreases as z becomes smaller, because the free-stream velocity decreases. This pressure gradient induces a spanwise flow directed away from the tip. Thus, there is a flow down the front face which interacts with the free-stream flow and produces a net deflection towards the ground plane. This interaction reinforces the bound vortex system which is swept around the cylinder and downstream. The result of this three dimensional effect is to increase considerably the local drag coefficient over that occurring in uniform flow as z/H → 0. Moreover, compared to uniform flow, the bound vortex system tends to delay separation and assist the flow to attain a lower minimum pressure coefficient before separating. The larger lateral suction is accompanied by an increase in the wake suction, which is responsible for higher local drag coefficients at the base. As said, the extent of this modification depends on the local shear flow gradient. For shear flow profiles of the boundary layer type, the ESDU provides – on the basis of H/D and the profile exponent α – a correction factor to the value of the drag coefficient in uniform flow. As z/H → 0, the correction factor increases significantly the local drag coefficient, especially for high slenderness ratios. The expression for such a correction factor, namely f_{sz} in the ESDU, is as follows:

$$f_{sz} = a + b\left(\frac{z}{H} - 0.7\right)^2 \tag{3.4}$$

where:

$$a = 0.8 + 0.2 * \exp\left(-1000\alpha^3\right) \tag{3.5}$$

$$\frac{b}{b_1} = 1.5\left(1 - \exp(-5.5\alpha)\right) \quad and \quad b_1 = 2.222\left(1 - \exp\left(-0.00303\left(\frac{H}{D}\right)^4\right)\right) \tag{3.6}$$

If H/D ≥ 6 and α = 0.16, $f_{sz}(z=0) = 2.4$, meaning that the drag coefficient at the base in shear flow is more than twice the corresponding value in uniform flow, due to a bound vortex system enhanced by vertical pressure gradients. The ESDU recommends to use such a correction factor even at transcritical Re, although most of the experiments have been carried out at lower Re.

Kawamura et al. (1984) carried out experiments on circular cylinders of different aspect ratios (H/D = 1, 2, 4, 6, 8) in turbulent boundary layer flows at Re = $3.2*10^4$.
The mean surface pressure distribution for the most slender case (H/D = 8) is reported in Figure 3.29. Close to the ground, the down-wash flow at stagnation decreases $C_p(0°)$ and the horseshoe vortices increase lateral suction and move downstream the separation line. All of that is in agreement with the ESDU recommendation. The tip effect, accompanied by high suction and downstream movement of the separation line, is evident at high levels.
According to Kawamura, the second islet of minimum pressure coefficient in the tip region, which is responsible for the high drag at about 1/3D (1/2D) from the top, is due to the attachment of trailing swirls, depicted in Figure 3.30 while they move downstream. As previously explained, longitudinal trailing vortices result from a coupling of the blow-down flow from the free-end and the separated up-wash flow along the side wall. The upward-directed flow sweeps the separated shear layers from intermediate heights towards the tip and rolls up in intense tip vortices with horizontal axis – counter rotating vortices – before passing downstream in a trailing vortex street (ESDU 96030).

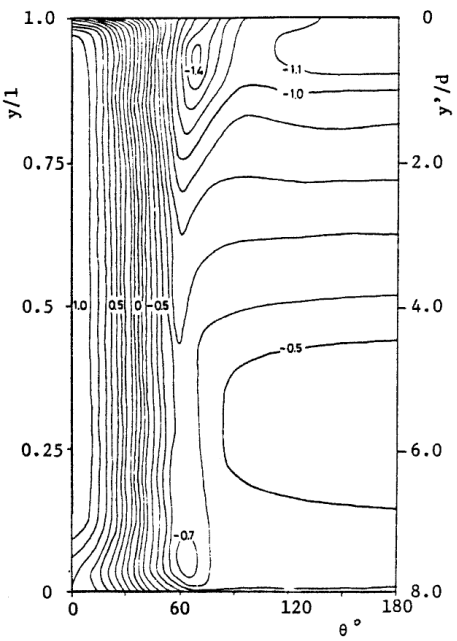

Figure 3.29 Surface pressure coefficients on a finite length circular cylinder H/D = 8 in turbulent boundary layer flow, Re = $3.2*10^4$. (Kawamura et al., 1984)

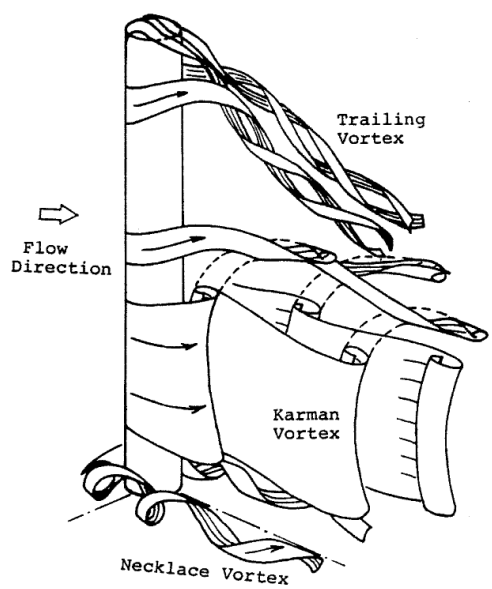

Figure 3.30 Model of the flow around a finite length circular cylinder H/D ≥ 2.5. (Kawamura et el., 1984)

Kawamura did not observe Karman vortex shedding near the free-end, because the free-end was dominated by the downwash. This issue, which will be addressed in the following, is questionable and it is contradicted by other authors.

The trailing vortices were observed by Kawamura even at low aspect ratios, while the formation of Karman vortex streets is suppressed below a critical H/D, which increases as the boundary layer grows thicker.
In contrast with Kawamura, Fox&West (1993) found that for low aspect ratios (H/D ≤ 4) longitudinal trailing vortices do not form. Consistently, there is no evidence of trailing vortices in the results by Uematsu et al. (1994) on cantilevers with aspect ratio in the range 1 to 4.
Sakamoto&Arie (1983) found a completely different flow structure, characterized by symmetric arch-type vortices at aspect ratios below 2.5. This is considered by the authors as the "critical" H/D value where the type of vortex shedding behind a circular cylinder changes from the Karman-type vortex to the arch-type vortex. However, the overall effect of changing the boundary layer height as well as the cylinder height or diameter is still not well understood and among different authors the critical aspect ratio varies in the range 1 to 7.

Below the tip region – which usually extends for two or three diameters and is characterized by high drag due to the high vorticity – the downwash flow leads to an increase in the wake pressure and then a reduced drag coefficient with respect to the two-dimensional situation (infinite cylinder). Therefore, the introduction of additional fluid from over the top relieves some of the negative base pressure. Consequently, the mean and fluctuating pressures below the tip region are lower than those obtained on a circular cylinder between two end plates and the mean drag coefficient decreases as H/D decreases (Okamoto&Sunabashiri, 1992).
As the distance from the tip increases, the strength of the downwash is reduced. This is consistent with what has been previously said about the size of the recirculation region in the wake. Because of that, Fox&West (1993) justified that, if the cantilever is sufficiently long (the value H/D ≥ 13 is chosen as reference to define a long cantilever), the C_D at low levels rises towards the infinite cylinder value. In their experiments they observed that such an infinite cylinder value (relatively high) is fully achieved at spanwise distance higher than 20 diameters from the top. Therefore, for longer circular cylinders, it is sufficient to consider that beyond 20 diameters from the top the conditions associated with the infinitely long circular cylinder are established. Only 3.5 diameters from the ground (Fox&West, 1990), the interference effect with the end-plate becomes significant and it is expressed by an increase in C_D.
Experiments by Fox&West are performed at subcritical Re (Re = $4.4*10^4$). The ESDU Data Items (ESDU 96030) observe that, at higher Re (Re > 10^6) the tip flow is weaker

and two-dimensional conditions are reached at smaller distance from the top than 20 diameters. Moreover, in presence of vertical velocity gradients and turbulence intensity due to a boundary layer, it can be supposed that the downwash is further weakened, so that the spanwise drag distribution at low levels tends to the high value of the two-dimensional drag coefficient, even at lower aspect ratios. This is a further explanation to the rise of C_D in Figure 3.28.

The weaker downwash in the wake in boundary layer flows compared to uniform flows is evident in Park&Lee' flow visualizations (2002). As a consequence of the weaker downwash, the recirculation bubble which normally develops on the rear side of the cylinder is smaller in boundary layer flows than in uniform flow. Therefore, at about middle height, the vortex formation region can move upstream, so that in boundary layer flows the vortices are formed closer to the cylinder, as shown by Figure 3.36.

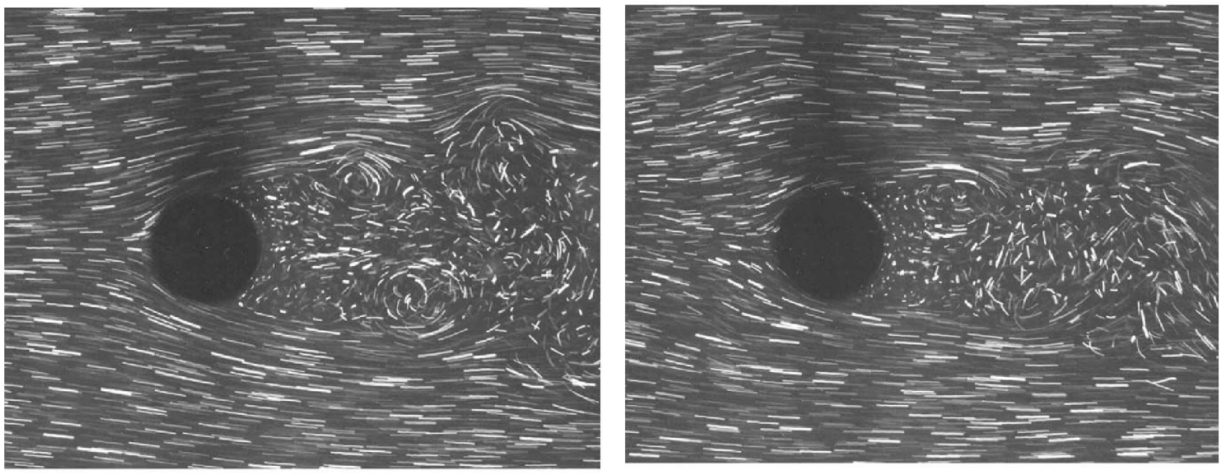

a) uniform flow *b) boundary layer flow*

*Figure 3.31 Top view of wake at middle height of the finite cylinder H/D = 6, Re = 2*10^4 (Park&Lee, 2002)*

The free-end condition, allowed by the absence of a physical boundary between the free stream pressure and the base pressure in the wake, has also an effect on eddy shedding. In particular, as explained by Zdravkovich (2003), the secondary flow over the tip is responsible for: 1) elongation of the eddy formation region, widening of the near-wake, decrease in Strouhal number; 2) displacement downstream of eddy shedding; 3) suppression of eddy shedding for small aspect ratios, so that the secondary flow becomes the primary flow.

A spanwise variation of the Strouhal number has been observed at first by Farivar (1981) at Re = 7*10^4 in uniform flow (Figure 3.32a). He found a cellular shedding

with three distinctive regions: a small top region ($z/H \geq 0.9$) characterized by low frequency of vortex shedding ($S_t \approx 0.08$), a middle region ($0.6 < z/H < 0.9$) characterized by higher frequency, but still lower than that for a classical wake flow ($S_t \approx 0.165$), and a lower region ($z/H \leq 0.6$) characterized by a Strouhal number equal to that for the classical wake flow ($S_t \approx 0.19$). On the basis of Roshko's experiments with a splitter plate placed in the wake of a cylinder parallel to the stream – which proved a decreases of the Strouhal number depending on the position of the splitter plate in the wake (Roshko, 1959) – and on the basis of Gerrard's theory on the length of the eddy formation region related to the frequency of vortex shedding (Gerrard, 1966), Farivar gathered the following explanation: the decrease in the Strouhal number in the tip region is due to a lengthening of the formation region, as it can be produced by a splitter plate; in the case of a cylinder with a free-end, the flow over the top enters the wake region and this entrainment causes a blockage in the wake preventing the interaction between vortices. Because of that, the formation region elongates and the frequency of vortex shedding is reduced. However, this does not explain the cellular shedding along the height.

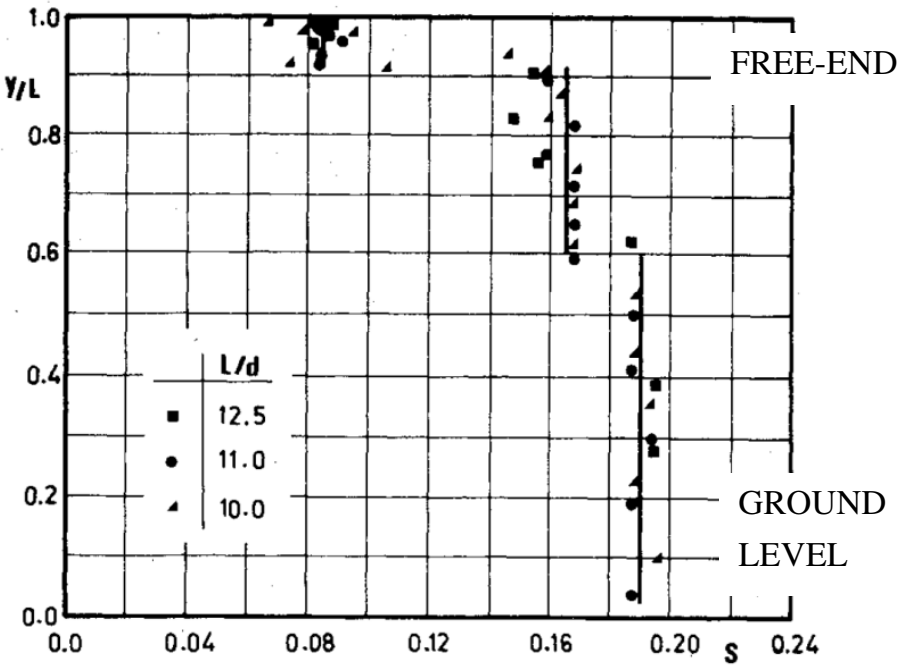

*Figure 3.32 Variation of the Strouhal number with height along a finite circular cylinder. Uniform flow, Re = Re = 7*104, H/D = 10, 11, 12.5 (Farivar, 1981)*

A decrease in the Strouhal number in the tip region of a finite length circular cylinder is also confirmed by Fox et al. (1993) and reported in Figure 3.32b. Cell-like structures were also detected in the wake by Ayoub&Karamcheti (1982), with vortex shedding occurring up to a short distance from the free-end.

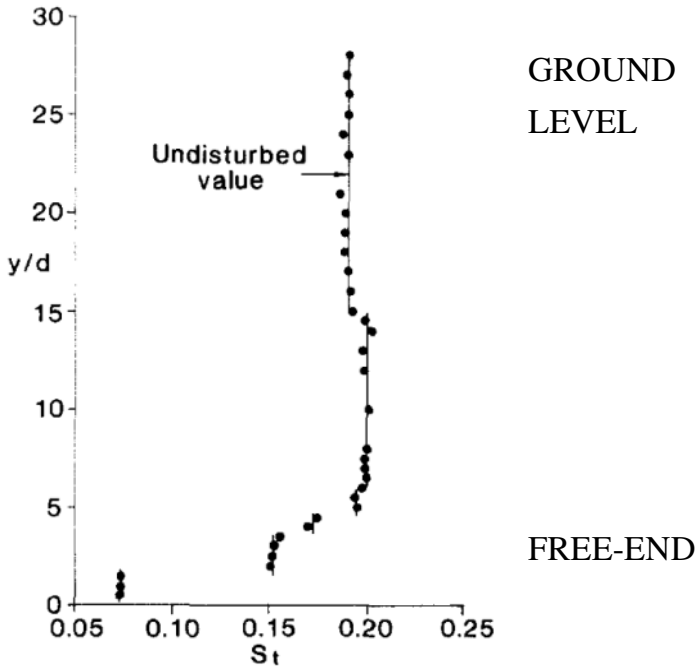

*Figure 3.33 Variation of the Strouhal number with height along a finite circular cylinder. Uniform flow, Re = Re = 4.4*10^4, H/D = 30 (Fox et al., 1993)*

Park and Lee (2000) deeply investigated the shedding frequency at the free-end, in comparison with Karman vortex frequency along the height. They tested three finite circular cylinders with aspect ratios 6, 10 and 13 respectively, in uniform flow at Re = 2*10^4. Near the free-end a peculiar spectral peak occurred at 24 Hz, which in the conditions of those tests corresponds to a reduced frequency nD/U = 24Hz*0.03m/10m/s = 0.072. At middle height the vortex shedding frequency depended on the aspect ratios and the following values were achieved: nD/U = 60*0.03/10 = 0.18 for H/D = 13; 0.16 for H/D = 10 and 0.14 for H/D = 6[2]. In the 2D conditions it resulted nD/U = 0.20, almost three times the reduced frequency in the tip region. The difference in the vortex shedding at middle height is attributed to the downwash flow along the central region of the wake. The strength of the downwash flow depends on the aspect ratio. It is interesting to note, instead, that the 24 Hz component is not modified by the different aspect ratio. However, several spanwise cells as those reported in Figure 3.32 are not observed by these authors. In agreement with Park&Lee's results, Luo et al. (1996) observed Strouhal numbers equal to 0.08 and 0.191 on their H/D = 8 cylinder at z/H = 0.95 and z/H ≤ 0.5 respectively, in uniform flow at Re = 3.33*10^4.

[2] In Park&Lee (2002) the same tests are repeated in atmospheric boundary layers and the vortex shedding frequencies and the vortex formation regions are lower.

Another wide study in uniform flow regarding the existence of big vortices generated around the free-end of a finite circular cylinder, whose frequency is much lower than the Karman vortex shedding frequency, is documented by Kitagawa et al. (1999, 2001, 2002) at Re = $2.5*10^4$ (Figure 3.34, Figure 3.35). Such vortices are called tip-associated vortices (TAV) and tend to vanish if the end conditions are modified, for example by a sufficiently large end disk. Kitagawa et al. (1999) found that with a circular disk over the free-end, with a diameter which is 20% more than the cylinder diameter, the tip-associated vortices are weakened; with an increase in the disk diameter up to 60% more than the cylinder diameter , the tip-associated vortices are almost vanished.

The tip-associated vortices are something different from the previously mentioned counter rotating vortices with horizontal axis – usually called tip vortices – which are produced by the interaction between the upward flow at the side of the cylinder and the downward flow over the tip and the rear and pass downstream in a steady street of longitudinal trailing vortices (Figure 3.30). The shedding frequency of tip-associated-vortices measured by Kitagawa is about 1/3 of the Karman vortex shedding frequency. The tip-associated-vortices possibly correspond to one of the cells detected by Farivar (1981) and others close to the tip of the circular cylinder. Detection of vortex shedding near the top is in contrast with the results, previously mentioned, by Okamoto&Yagita (1973, 1984) and Kawamura et al. (1984). They did not observe vortex shedding near the top, but only stationary longitudinal trailing vortices (Figure 3.30).

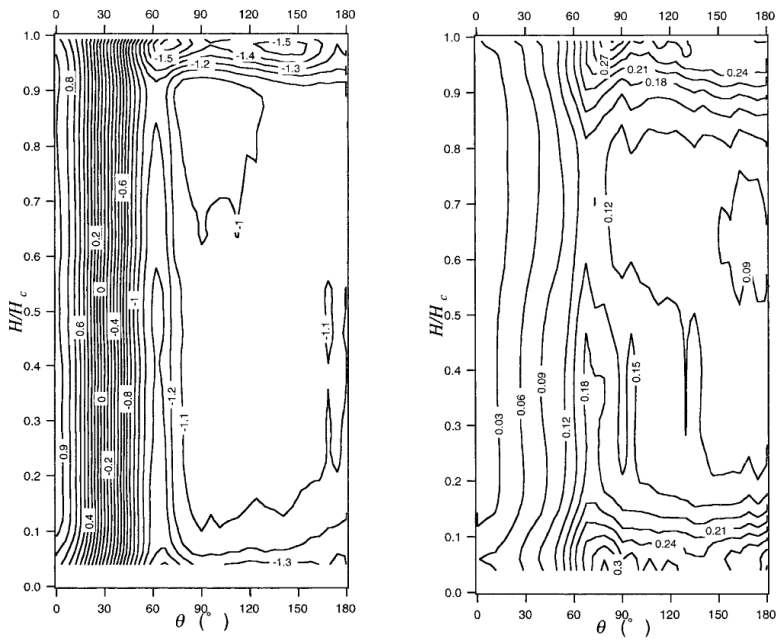

Figure 3.34 Pressures on a finite cylinder, uniform flow, H/D = 25, Re = $2.5*10^4$
a) $C_{p,m}$; b) $C_{p,\sigma}$; (Kitagawa et al., 2001)

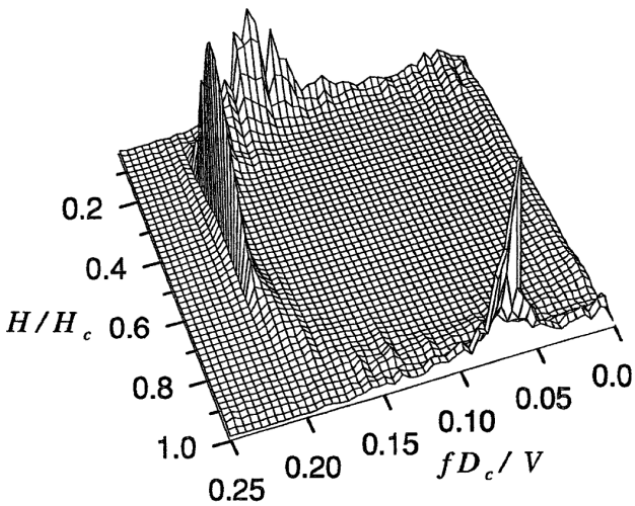

*Figure 3.35 Power spectra of fluctuating pressures at 90°: existence of tip-associated-vortices, uniform flow, H/D = 25, Re = 2.5*10^4 (Kitagawa et al., 2001).*

Aeroelastic tests by Kitagawa et al. (1999) studied the so-called end-cell-induced-vibrations (ECIV), which are similar to the vortex-induced-vibration (VIV), but they occur at a wind speed a few times higher than the threshold wind speed of VIV. Tip-associated-vortices are found to be the cause of ECIV. In fact, according to Kitagawa, ECIV could not be generated by sub-harmonic oscillations of the Karman vortex shedding, although they also occur at a flow velocity a few times higher than that for VIV. The difference is that ECIV tend to vanish with modification of the flow around the free-end, for example by using a disk plate. This would not happen if ECIV were generated by sub-harmonic oscillations and not by the tip-associated vortices.

Three dimensional effects on the flow around circular cylinders have been studied in recent years by numerical simulations. A few of them have been mentioned before. Some important ones are cited in the following. However, many of them are only for short aspect ratio cylinders. In particular, a large eddy simulation of a finite cylinder H/D = 2.5 at Re = 4.3*10^4 was performed by Fröhlich&Rodi (2004), who demonstrated the existence of tip vortices and an arch vortex in the average flow downstream of the free end. Similar results were obtained by Lee et al. (2007). Afgan et al. (2006) presented LES of the flows studied by Park&Lee (2000), i.e. circular cylinder with H/D = 6 in uniform flow at Re = 2.0*10^4. Palau-Salvador et al. (2010) made LES of their own experimental cases with H/D = 2.5 at Re = 4.3*10^4 and H/D = 5 at Re = 2.2*10^4. Krajnovic (2011), previously mentioned in the description of the near-wake flow, used LES to explore both the instantaneous and the time-averaged flows around a relatively tall cylinder (H/D = 6) in uniform flow at Re = 2*10^4.

3.6 Bi-stable flows in literature

Bistable flow conditions around isolated circular cylinders in the critical range of Re (section 3.2) represent a well-known and interesting fluid-dynamic phenomenon, but without any relevant application in the design of structures. As previously explained, the physical reason lies in the transition from laminar to turbulent boundary layer, which occurs on one side only of the cylinder. The transition to turbulent conditions is governed by the Reynolds number. The bistable regime occurs in a very small range of Re, just before Re_{cr}. Most of the structures are far beyond this regime. Moreover, the bistable phenomenon is extremely sensitive not only to Re, but also to any flow disturbance such as turbulence of the incoming flow and cylinder surface roughness.
Bistable flow conditions around circular cylinders are much more common in side-by-side configurations of cylinders in pair. In this case, the bi-stability is regarded as a phenomenon of interaction between cylinders and it can be of importance in the structural design. The fluid behaviour is primarily a function of the centre-to-centre transverse pitch ratio (T/D). Reynolds effects for the side-by-side configuration exist, but they are less prominent than, for example, the tandem configuration. Depending on T/D, three different flow patterns are possible for the side-by-side configuration (Zdravkovich, 2003):

- single-bluff-body behaviour at small pitch ratios (approximately 1.0 < T/D < 1.1-1.2, Figure 3.36a): the single eddy street is formed behind both cylinders, which appear as a single bluff body with a weak flow through the gap;
- a biased flow pattern at intermediate pitch ratios (approximately 1.1-1.2 < T/D < 2.0-2.2, Figure 3.36b): narrow and wide wakes are formed behind two identical cylinders. The gap flow forms a jet biased towards the narrow wake. The biased gap flow is bistable, and may intermittently switch to either side;
- coupled, parallel vortex streets at high pitch ratios (approximately T/D > 2.0-2.5, Figure 3.36c): both wakes are equal in size and eddy shedding is synchronized in frequency and phase. The predominant out-of-phase coupling produces two eddy streets, which mirror each other relative to the gap axis.

A recent review paper by Sumner (2010) further describes the asymmetrical or biased flow pattern at intermediate values of T/D for two side-by-side circular cylinders: the asymmetrical flow pattern is characterized by a gap flow biased towards one of the two cylinders. The cylinder towards which the flow is biased has a narrow near-wake, higher-frequency vortex shedding, and a higher drag coefficient, while the other

cylinder has a wider near-wake, lower-frequency vortex shedding, and a lower drag coefficient. Because of that, the two modes “narrow wake” and “wide wake” can be identified. The deflection of the biased gap flow varies with T/D. The trend is toward a smaller degree of deflection with increasing T/D. In some cases, the biased flow pattern switches intermittently from being directed towards one cylinder to the other, and the flow pattern is termed bistable. This ‘‘flip-flopping’’ of the gap flow direction and wake sizes occurs spontaneously and irregularly, but between switchovers the flow remains stably biased to one of the cylinders for long durations (perhaps a few orders of magnitude larger than the vortex shedding period). The bistable characteristic is not caused by misalignment of the cylinders or other extraneous influences, but is an intrinsic property of the flow.

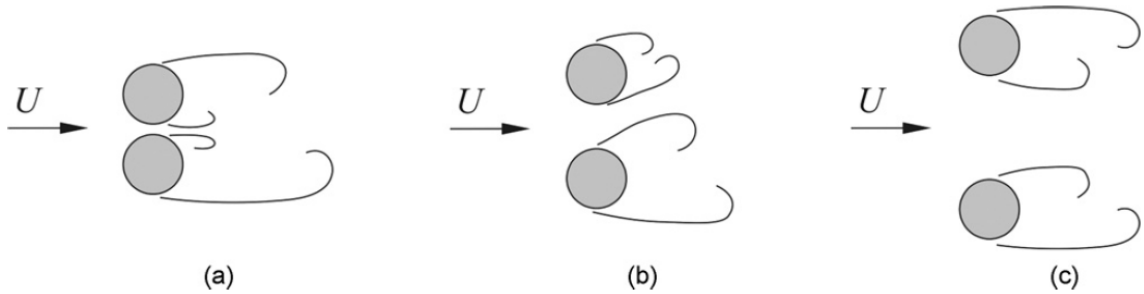

Figure 3.36 Flow patterns for two side-by-side circular cylinders: a) single-bluff-body behaviour; b) biased flow pattern; c) parallel vortex streets (Sumner, 2010);

Mahbub Alam et al. (2003) applied a wavelet analysis in order to detect the frequency of vortex shedding in the two modes (narrow wake, wide wake) and the switching phenomenon.

Three modes of flow, associated with wider wake, symmetric wake and narrow wake are described by Mahbub Alam&Meyer (2011) and sketched in Figure 3.37. The formation and burst of a separation bubble when the gap flow is biased towards one of the two cylinders can even produce a quadri-stable flip-flopping flow regime. A typical lift force signal is shown in Figure 3.38.

Zdravkovich (2003) stresses the paradox of Figure 3.36b, which shows the bistable biased gap flow. The paradox is due to two special features: the first is that an entirely symmetrical oncoming flow leads to the asymmetric narrow and wide wakes behind the two identical side-by-side cylinders. The second is that a uniform and stable flow induces a non-uniform and random bistable flow. The origin of bistable biased flow has been attributed to various causes, but still remains unresolved.

Ishigai et al. (1972) suggested that the Coanda effect is responsible for the biased gap flow. The Coanda effect is observed when a jet tangentially attached to a curved surface becomes deflected by following the surface. According to this definition, it is essential to have a rounded surface. Because of that, Bearman&Wadcock (1973) proved that the Coanda effect could not be the reason; the biased gap flow also appeared by using side-by-side flat plates.

Zdravkovich&Pridden (1977) and Zdravkovich (1987) also observed stable narrow and wide wakes on the upstream and downstream cylinders in staggered arrangement, respectively. As the side-by-side arrangement is approached, the distinction persists so that one cylinder remained upstream with a narrow wake, and the other downstream, with a wide wake. In a side-by-side configuration the asymmetric flow structure is preserved, but it becomes bistable because neither of the side-by-side cylinders is upstream nor downstream. Zdravkovich (2003) concludes that the flow structure consisting of two identical wakes appears to be intrinsically unstable and hence impossible.

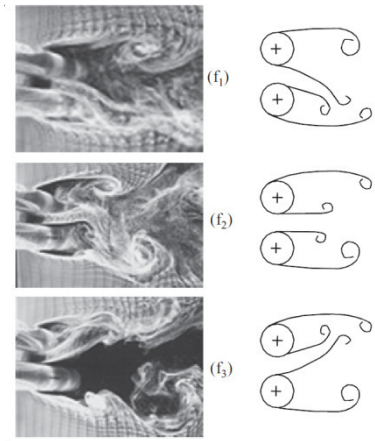

Figure 3.37 Tri-stable flow (T/D = 0.4) (Mahbub Alam&Meyer, 2011)

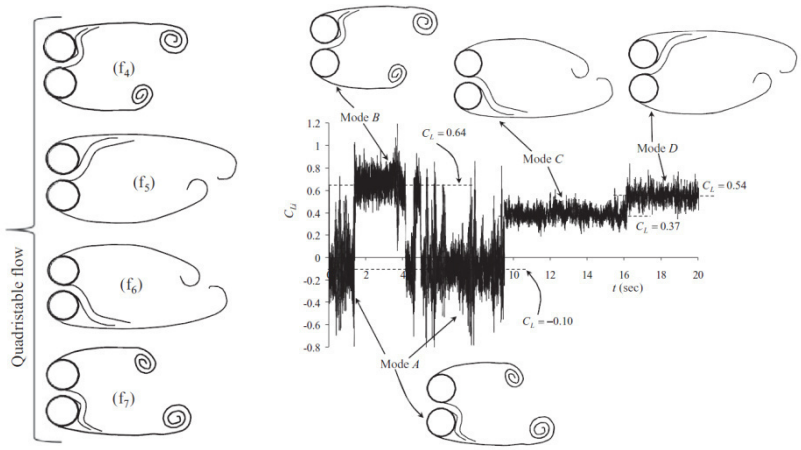

Figure 3.38 Quadri-stable flow due to formation and burst of a separation bubble (T/D = 0.13) (Mahbub Alam&Meyer, 2011)

This Dissertation addresses the case of only one isolated circular cylinder. However, a similar bistable phenomenon of interaction like the one previously described occurs in the wake between different compartments of the single cylinder, which are separated by stiffening rings. This effect is addressed in Chapter 5.